





รายงานวิจัยฉบับสมบูรณ์

โครงการ

 Fe_3O_4 อนุภาคแม่เหล็กนาโน/รีดิวซ์กราฟีนออกไซด์ คอมโพสิตนาโน: การประยุกต์ใช้เป็นเซ็นเซอร์ ตรวจวัดสารปนเปื้อนในอาหารและเซลล์เชื้อเพลิงชีวภาพแบบเอ็นไซม์ที่มีประสิทธิภาพสูง (Fe_3O_4 magnetic nanoparticles/reduced graphene oxide nanocomposite: Application to food contaminant sensors and high performance enzymatic biofuel cells)

โดย ผศ.ดร.รุ่งทิวา ภู่อาภรณ์ และคณะ

เมษายน 2562

รายงานวิจัยฉบับสมบูรณ์

โครงการ

 Fe_3O_4 อนุภาคแม่เหล็กนาโน/รีดิวซ์กราฟีนออกไซด์ คอมโพสิตนาโน: การประยุกต์ใช้เป็นเซ็นเซอร์ ตรวจวัดสารปนเปื้อนในอาหารและเซลล์เชื้อเพลิงชีวภาพแบบเอ็นไซม์ที่มีประสิทธิภาพสูง (Fe_3O_4 magnetic nanoparticles/reduced graphene oxide nanocomposite: Application to food contaminant sensors and high performance enzymatic biofuel cells)

ผู้วิจัย

ผศ.ดร.รุ่งทิวา ภู่อาภรณ์ หลักสูตรวิศวกรรมชีวภาพ คณะวิศวกรรมศาสตร์ มหาวิทยาลัยเทคโนโลยีพระจอมเกล้าธนบุรี

สนับสนุนโดยสำนักงานกองทุนสนับสนุนการวิจัยและสถาบันวิจัยแสงซินโครตรอน (องค์การมหาชน)
(ความเห็นในรายงานนี้เป็นของผู้วิจัย สกว.ไม่จำเป็นต้องเห็นด้วยเสมอไป)

รหัสโครงการ RSA5980073

ชื่อโครงการ ${\sf Fe_3O_4}$ อนุภาคแม่เหล็กนาโน/รีดิวซ์กราฟีนออกไซด์ คอมโพสิตนาโน: การประยุกต์ใช้

เป็นเซ็นเซอร์ตรวจวัดสารปนเปื้อนในอาหารและเซลล์เชื้อเพลิงชีวภาพแบบเอ็นไซม์ที่

มีประสิทธิภาพสูง

ชื่อนักวิจัย ผศ.ดร.รุ่งทิวา ภู่อาภรณ์ หลักสูตรวิศวกรรมชีวภาพ คณะวิศวกรรมศาสตร์

มหาวิทยาลัยเทคโนโลยีพระจอมเกล้าธนบุรี

E-mail Address: rungtiva.pal@kmutt.ac.th

ระยะเวลา 3 ปี

บทคัดย่อ

งานวิจัยนี้นำเสนอแนวทางใหม่ในการตรึงเอ็นไซม์แบบ self-assembly ระหว่างกลูโคสออกซิเดส (GOD) และรีดิวซ์กราฟีนออกไซด์ (rGO) ที่จับกับอนุภาคแม่เหล็กนาโน (Fe₃O₄ NPs) แบบโควาเลนท์ และนำไป ปรับปรุงบนขั้วแม่เหล็กชนิดพิมพ์สกรีน (MSPCE) เพื่อสร้างเป็นเซ็นเซอร์ตรวจวัดกลูโคสที่มีความจำเพาะ และความเสถียรโดยอาศัยการตรวจวัดทางเคมีไฟฟ้าโดยตรง คอมโพสิตนาโน Fe₃O₄/rGO เป็นที่จดจำว่า ้มีความสามารถในการเพิ่มพื้นที่ผิวซึ่งทำให้การตรึงเอ็นไซม์เพิ่มขึ้น ช่วยในการส่งผ่านอิเล็กตรอนระหว่าง เอ็นไซม์และพื้นผิวอิเล็กโทรดดีขึ้น และมีคุณสมบัติความเป็นแม่เหล็ก ลักษณะทางกายภาพและ คุณสมบัติทางเคมีไฟฟ้า ของ Fe₃O₄/rGO/GOD ได้ถูกวิเคราะห์โดย scanning electron microscopy (SEM), Fourier transform infrared spectroscopy (FTIR), Raman spectroscopy, cyclic voltammetry (CV) และ amperometry จากการทดลองพบว่าขั้วไฟฟ้าที่ถูกปรับปรุงนี้ อิเล็กตรอนมี การถ่ายโอนได้โดยตรงอย่างรวดเร็วโดยมีค่าคงที่การถ่ายโอน (electron transfer rate constant) k_{s} เป็น 13.78 $\mathrm{s}^{\text{-}1}$ นอกจากนี้ไบโอเซ็นเซอร์แสดงให้เห็นถึงการตอบสนองทาง amperometric ต่อกลูโคส อย่างรวดเร็ว (3 s) และมีค่า linear range เป็นช่วงกว้างจาก 0.05 ถึง 1 mM มีค่า detection limit ที่ ต่ำถึง 0.1 μ M ขณะที่ signal to noise ratio เป็น 3 (S/N=3) มีความว่องไวในการตรวจวัดที่ดี (5.9 μ A/mM) เซ็นเซอร์ที่พัฒนาได้นี้มีความเสถียรสูง มีความสามารถในการ reproducibility ที่ดี และมี ความจำเพาะสงและตรวจวัดได้ที่ศักย์ไฟฟ้า -0.45 V

นอกจากนี้ได้มีการสร้างเซลล์เชื้อเพลิงชีวภาพแบบเอ็นไซม์ (EBFC) ที่อาศัยกลูโคสเป็นเชื้อเพลิง ชนิดไม่มีเมมเบรนและไม่ใช้ตัวกลางที่ทำงานได้ในสภาวะร่างกาย (pH 7.0 และอุณหภูมิ 37 °C) EBFC ต้นแบบนี้สร้างจากการใช้คอมโพสิตนาโน Fe $_3$ O $_4$ /rGO ในการตรึงกับเอ็นไซม์ glucose oxidase (GOD) เป็น bioanode และตรึงกับเอ็นไซม์ bilirubin oxidase (BOD) เป็น biocathode ซึ่ง EBFC bioelectrodes ที่สร้างขึ้นนี้ไม่ต้องใช้ตัวจับหรือสารยึดเกาะใดๆในการตรึงกับเอ็นไซม์และเป็นการ รายงานครั้งแรกของ EBFC ที่ใช้คุณสมบัติ superparamagnetic ของFe $_3$ O $_4$ NPs ประสิทธิภาพของ EBFC ได้ถูกศึกษาและผลที่ดี จากการทดสอบEBFC พบว่าค่า maximum power density เป็น 73.7 μ W cm $^{-2}$ และ open circuit voltage (OCV) มีค่า+0.63 V เมื่อใช้กลูโคสความเข้มข้น 5 mM ใน สภาวะร่างกาย

จากนั้นได้มีการพัฒนาเซ็นเซอร์ทางเคมีไฟฟ้าแบบใช้แล้วทิ้งแบบใหม่ในการตรวจวัดอย่างรวดเร็ว ของสารแรคโตพามีน (RAC) โดยอาศัยการปรับปรุงขั้วแม่เหล็กไฟฟ้าแบบพิมพ์สกรีนด้วยอนุภาคแม่เหล็ก นาโน เหล็กออกไซด์ติดบนรีดิวซ์กราฟีนออกไซด์ (Fe $_3$ O $_4$ /rGO) การวิเคราะห์ รูปร่างลักษณะ โครงสร้าง และส่วนประกอบของนาโนคอมโพสิตทำโดยใช้ TEM, x-ray absorption spectroscopy (XANES) และ x-ray photoelectron spectroscopy (XPS) ผลการศึกษาจาก XANES แสดงให้เห็นว่านาโนคอมโพสิต ที่เตรียมได้แสดงพฤติกรรมการเป็นแม่เหล็ก โดยที่โครงสร้างคั้งเดิมของ Fe $_3$ O $_4$ NPs ถูกแสดงหลังจากที่ ติดอยู่บน rGO สำเร็จแล้ว ผลจาก XPS ยืนยันส่วนประกอบทางเคมีของ GO, GO ที่ติดด้วย Fe $_3$ O $_4$ และ นาโนคอมโพสิตที่ถูกรีดิวซ์ด้วยกลูโคสเป็น Fe $_3$ O $_4$ rGO การศึกษาคุณลักษณะทางเคมีไฟฟ้า และการเร่ง ทางไฟฟ้าของขั้วไฟฟ้าที่ถูกปรับปรุงทำโดยใช้เทคนิค CV และ differential pulse voltammetry (DPV) รวมถึงได้มีการศึกษาค่าที่เหมาะสมของปัจจัยที่มีผลต่อประสิทธิภาพของเซ็นเซอร์ พีคของกระแสที่ได้จาก เทคนิค DPV เพิ่มขึ้นเป็นเส้นตรงกับการเพิ่มขึ้นของความเข้มข้นของ RAC นอกจากนี้เซ็นเซอร์ที่ได้มีค่า การตรวจวัดได้ในช่วงความเข้มข้น 0.05–10 และ 10–100 μ M โดยที่ detection limit เป็น 13 nM (S/N=3) เนื่องจากนาโนคอมโพสิต Fe $_3$ O $_4$ rGO ช่วยในการถ่ายโอนอิเล็กตรอน และเพิ่มความไวในการ ตอบสนองของเซ็นเซอร์ เซ็นเซอร์ที่ใช้แล้วทิ้งที่เสนอในงานวิจัยนี้แสดงให้เห็นถึงความไวในการตอบสนอง ที่ดี มีความเสถียร และทำซ้ำได้รวมถึงใช้ในการตรวจวัดในตัวอย่างเนื้อหมูจริงได้เป็นอย่างมีประสิทธิภาพ

คำหลัก เซ็นเซอร์ทางเคมีไฟฟ้า เซลล์เชื้อเพลิงชีวภาพแบบเอ็นไซม์ กลูโคสเซ็นเซอร์แบบตรง แรคโต พามีน รีดิวซ์กราฟีนออกไซด์ เหล็กออกไซด์อนุภาคแม่เหล็กนาโน Project Code RSA5980073

Project Title Fe₃O₄ magnetic nanoparticles/reduced graphene oxide nanocomposite:

Application to food contaminant sensors and high performance

enzymatic biofuel cells

Investigator Assist. Prof. Dr. Rungtiva Poo-arporn, Biological Engineering Program,

Faculty of Engineering, King Mongkut's University of Technology

Thonburi

E-mail Address rungtiva.pal@kmutt.ac.th

Project Period 3 years

Abstract

A novel approach of the immobilization of a highly selective and stable glucose biosensor based on direct electrochemistry was fabricated by a self-assembly of glucose oxidase (GOD) on reduced graphene oxide (rGO) covalently conjugated to magnetic nanoparticles (Fe₃O₄ NPs) modified on a magnetic screen-printed electrode (MSPCE). The Fe₃O₄/rGO nanocomposite has remarkable enhancement in large surface areas, is favorable for enzyme immobilization, facilitates electron transfer between enzymes and electrode surfaces and possesses superparamagnetism property. The morphology and electrochemical properties of Fe₃O₄/rGO/GOD were characterized by scanning electron microscopy (SEM), Fourier transform infrared spectroscopy (FTIR), Raman spectroscopy, cyclic voltammetry (CV) and amperometry. The modified electrode was a fast, direct electron transfer with an apparent electron transfer rate constant (k_s) of 13.78 s⁻¹. The proposed biosensor showed fast amperometric response (3 s) to glucose with a wide linear range from 0.05 to 1 mM, a low detection limit of 0.1 **µ**M at a signal to noise ratio of 3 (S/N=3) and good sensitivity (5.9 μ A/mM). The resulting biosensor has high stability, good reproducibility, excellent selectivity and successfully applied detection potential at -0.45 V.

Moreover, an enzymatic biofuel cell (EBFC) based on a membraneless and mediatorless glucose enzymatic fuel cell system was constructed for operation in physiological conditions (pH 7.0 and temperature 37 °C). The new platform EBFC made of Fe₃O₄/rGO nanocomposite was used for the immobilization of glucose oxidase (GOD) as bioanode and bilirubin oxidase (BOD) as biocathode. The EBFC bioelectrodes were fabricated without binder or adhesive agents for immobilized enzyme and the first EBFC using superparamagnetic properties with Fe₃O₄ NPs has been reported. The performance

of the EBFC was evaluated with promising results. In EBFC tests, the maximum power density of the EBFC was 73.7 μ W cm⁻² and an open circuit voltage (OCV) as +0.63 V with 5 mM of glucose concentration for the physiological condition of humans.

Then, new disposable electrochemical sensor for rapid determination of ractopamine (RAC) is developed based on the use of MSPCE modified with Fe₃O₄/rGO. Morphology, structure and composition of nanocomposites were characterized by TEM, x-ray absorption spectroscopy (XANES) and x-ray photoelectron spectroscopy (XPS). XANES results indicated that the prepared nanocomposites exhibited the magnetic behavior, and the original structure of Fe₃O₄ NPs was displayed after being successfully doped on the rGO. XPS was used to confirm the chemical compositions of GO, GO doped with Fe₃O₄ and Fe₃O₄/rGO reduced by glucose. The electrochemical and electrocatalytic characteristics of the modified MSPCE were recorded using CV and differential pulse voltammetry (DPV) and the factors that affected the performance of the sensor were also optimized. The peak currents obtained by DPV increased linearly with the increasing of the concentration of RAC and the sensor had a detection range over the concentration ranges of 0.05-10 and 10-100 μ M, with a detection limit of 13 nM (S/N=3). Due to the Fe₃O₄/rGO promoting the electron transfer, and raising the sensitivity of the sensor, the proposed disposable sensor displayed a good sensitivity, stability and reproducibility and robust operation in spiked real pork samples.

Keywords: Electrochemical sensors, Enzymatic biofuel cell, Direct glucose sensor, Ractopamine, Reduced graphene oxide, Iron oxide magnetic nanoparticle

Executive Summary

1. Project title

Thai: Fe₃O₄ อนุภาคแม่เหล็กนาโน/รีดิวซ์กราฟีนออกไซด์ คอมโพสิตนาโน: การ

ประยุกต์ใช้เป็นเซ็นเซอร์ตรวจวัดสารปนเปื้อนในอาหารและเซลล์เชื้อเพลิง

ชีวภาพแบบเอ็นไซม์ที่มีประสิทธิภาพสูง

English: Fe₃O₄ magnetic nanoparticles/reduced graphene oxide

nanocomposite: Application to food contaminant sensors and high

performance enzymatic biofuel cells.

2. Principal investigator / Department / Faculty / Institute / Telephone /Fax / e-mail

ผศ.ดร.รุ่งทิวา ภู่อาภรณ์ สังกัด หลักสูตรวิศวกรรมชีวภาพ คณะวิศวกรรมศาสตร์ มหาวิทยาลัยเทคโนโลยีพระจอมเกล้าธนบุรี

โทรศัพท์ 02-470-9393 โทรสาร 02-470-9391

มือถือ 086-710-2013

E-mail: rungtiva.pal@kmutt.ac.th

3. สาขาวิชาที่ทำการวิจัย Chemical sensors and biosensors, Nanobioengineering

4. Total budget 1,500,000 baht

5. Project duration 3 year since 15 August 2016 – 15 April 2019

6. Introduction to the research problem and its significance

Every year, the global energy demand increases. While petroleum products currently supply much of this demand, the increasing difficulty of sustaining supply and the problems associated with pollution and global warming are acting as the major impetuses for research into alternative renewable energy technologies. The developed world is becoming increasingly dependent of energy consumption and the pressure for efficient and green energy sources has increased dramatically over the past years. To address this issue, in the past decades, researchers and companies worldwide have created new possibilities of designing efficient energy conversion devices. Among a wide range of technologies being developed, fuel cells offer a possible (and partial) solution to this problem. Typically, the fuel required for conventional fuel cells is either hydrogen or methanol; some alternative fuel cells running on other fuels such as hydrocarbons have been developed. Nowadays, fuel cells represent a promising alternative for energy production with many advantages compared to combustion of fossil energy or nuclear power. They provide another mode of electric energy generation which is based on the transformation of chemical energy directly into electricity via

redox reactions or chemical reactions without going through the combustion process. This leads to higher efficiency as well as reducing the environmental impact. A fuel cell usually operates with two catalytic electrodes immersed in an electrolyte where the anode oxidizes the "fuel" (e.g. hydrogen or alcohols) and the cathode catalyzes, in most cases, the reduction of oxygen. The operation of fuel cells is similar to that of batteries but, unlike batteries, fuel cells can be used continuously without recharging. This eliminates the limited capacity of the battery out. In addition, the battery terminals react when it is charging or discharging. However, for the fuel cells, the need for noble metals such as platinum to catalyze the reactions that convert chemical energy into electricity is a limiting factor, as these metals are expensive, scarcely available and exhaustible. In the last century, technologies have emerged in which they are replaced by whole microorganisms or parts of these latter, leading to microbial, mitochondrial or enzymatic. Biofuel cells (BFCs) are a special type of fuel cells which use natural enzyme or microorganisms as a catalyst or directly transform chemical energy to electrical energy via electrochemical reaction involving biochemical pathways. Enzyme-based biofuel cells (EBFCs) utilize enzymes to catalyze chemical reactions in order to convert chemical energy into electrical energy, replacing traditional expensive metal catalysts such as platinum employed in conventional fuel cells. Furthermore, EBFCs can generate electricity under mild conditions such as at ambient temperatures, under physiological conditions, and neutral pH. Fuel flexibility and the use of a clean and renewable catalyst through the oxidation of renewable energy sources without greenhouse gas emissions or environmental pollution, make them not only useful for biomass conversion but also as potential alternative power sources for in vivo applications for implantable biomedical devices such as miniaturized sensors, transmitters, and artificial organs. To date, the vast majority of EBFCs are based on the enzymatic oxidation of glucose at the bioanode and the oxygen reduction at the biocathode. Usually, enzyme immobilization occurs by either chemical or physical processes such as covalent binding [1], cross-linking [2], sol-gel [3], mesoporus [4] and entrapment in polymer [5].

However, there are currently no EBFCs products available in the commercial market due to the lack of efficient enzyme immobilization techniques, the production of electrical energy is not as much as it should have been. The rate of electron transfer between the redox center of biocatalysts and the underlying electrodes is very slow, leading to low efficiency and small power output of EBFCs. The enzyme on the electrode surface usually does not achieve significant electron transfer between the immobilized enzymes and the current collector or the electrode, mostly because of the

electrical insulation of the active sites of the enzyme by the surrounding protein shells. To solve this problem, great efforts have been made to improve the direct or mediated electron transfer reactions of the enzymes by immobilizing them onto various interfaces or by using redox mediators. In order to improve the electron transfer rate between the enzyme and the electrode surface, some of the new trends in the catalyst design for EBFCs include the incorporation of nanoscale materials and metallic nanoparticles into the bioelectrode structure [3, 6-9]. The low stability of enzymes and their low turnover numbers are still the limiting factors for constructing applicable EBFCs. Nanomaterials have generated unprecedented interest due to their unique physical and chemical properties and optimal environment for the immobilization of proteins and other biological molecules, providing larger surface area that enables incorporation of larger enzyme loading. Additionally, these nanomaterials can significantly improve the bioelectrode electroactivity as they provide more efficient electrical contact with the enzyme active sites.

Graphene, a single layer of carbon material with a two-dimensional honeycomb sp² carbon lattice, possesses many unique features such as large surface area, good electrical, thermal, and mechanical properties. These unique properties are the reasons why graphene has been widely employed for various applications such as field-effect transistors [10], gas sensors [11-12], electromechanical sensors -biosensor [13-15], nanoelectronics [16], batteries [17-18], supercapacitors [19] and hydrogen storage [20]. In addition, varieties of hybrid materials between graphene and other materials such as polymers, metals, metal oxides and even carbon nanotubes with new functions are promising for utilization in various applications. However, the dissolution and biocompatibility of the graphene may restrict their practical applications [21-22]. Different types of materials have been used to immobilize enzymes and to improve the enzymatic activity. Graphene oxide (GO) is chemically modified graphene containing oxygen functional groups such as epoxides, alcohols, and carboxylic acids [23] and chemical analysis shows the carbon to oxygen ratio is approximately three to one [24]. Recently, GO has received a great deal of attention because it readily exfoliates as single sheets in water. Since, in its as-oxidized state, numerous oxygen functional groups of GO render it too electrically insulating for using as a conductance-based sensor. Thus, reduced graphene oxide (rGO) is both conductive and has chemically active defect sites making it a promising candidate as the active material in sensors [25-26].

Exploiting magnetic nanoparticles (Fe_3O_4 NPs) as a special bimolecular immobilizing carrier is the focus of this research. Due to its special properties, magnetic

NPs have been used in immunology [27] and drug delivery [28-29]. Due to its good biocompatibility, strong superparamagnetism, low toxicity, large surface-to-volume ratio, high surface reaction activity, strong adsorption ability to immobilize desired biomolecules and easy preparation process, magnetic NPs have been used to immobilize enzyme in different matrices [30-34]. The use of magnetic NPs for bioelectrodes purposes is based on their enhanced surface area, high catalytic activity, as well as their comparable size with some of the oxidoreductase enzymes employed in biofuel cells thus decreasing the electron transfer distance and, as a result, facilitating this process. The integration of magnetic NPs and rGO with enzymes may offer a hybrid nanocomposite with synergistic properties improving the electrical contact with the enzyme active sites and, consequently, fuel oxidation. Therefore, Fe₃O₄ magnetic NPs formed on the surface of rGO may provide more surface area and good biocompatibility for enzyme immobilization. Integration of Fe₃O₄ and rGO into a nanocomposite has recently become a popular topic of research because of its new and enhanced functionalities, therefore, it holds a great promise for wide-range of applications in catalysis, biomedical field, adsorption and separation, etc. [35-38].

In this research work, the possibility of employing Fe₃O₄/rGO nanocomposite as a potential candidate for the construction of EBFCs is proposed. We designed and developed EBFCs using glucose as a fuel by using nanocomposites and a group of enzymes, glucose oxidase and bilirubin oxidase to increase the immobilization of the enzyme, enhance the efficiency of power generation, improve the stability of the electrode and extend the lifetime of the system. Initially, Fe₃O₄/rGO nanocomposite were chemically synthesized and characterized by surface and chemical characterization techniques. In this work, we characterized the nanocomposite by using synchrotronbased x-ray photoelectron spectroscopy (XPS), x-ray absorption near-edge structure (XANES), extended x-ray absorption fine structure (EXAFS), scanning electron microscopy (SEM), Fourier transform infrared spectroscopy (FT-IR) and Vibrating sample magnetometer (VSM). Following the characterization, Fe₃O₄/rGO nanocomposite were employed to fabricate the anode and cathode in the EBFC. Due to the specific catalytic activity of these enzymes, the proton exchange membrane is eliminated to facilitate the fabrication process. Fe₃O₄/rGO nanocomposite not only has a great potential as it increases the immobilization of the enzymes but also can be used to catalyze hydrogen peroxide which is a byproduct from glucose oxidation at anode, hence our work was the first reported employing Fe₃O₄ based rGO for EBFCs application. We investigated the electrochemical performance of glucose EBFCs by using electrochemical methods. After fabrication of the nanocomposite based membraneless EBFCs, the maximum power density was quantified. This EBFCs may replace the batteries in medical devices applications in the future.

Herein, by applying different kinds of important compounds as representative examples, the usefulness of the nanocomposite for sensing and biosensing purposes were strongy demonstrated. With the advantages of the magnetism, conductivity, biocompatibility as well as good dispersibility in polar solvents of the Fe_3O_4/rGO nanocomposite, it could be facilely adhered to the electrode surface by magnetically controllable assembling and be beneficial to achieve the direct redox reactions and electrocatalytic behaviors of GOx immobilized into the nanocomposites. Hence, a direct electrochemical biosensing for glucose determination was developed based on $Fe_3O_4/rGO/GOD-MGCE$ bioanode.

Moreover, the potential applicability of the nanocomposite modified magnetic screen-printed electrode (MSCPE) as a novel disposable electrochemical sensing platform for food contaminants was investigated. Food safety has become a global concern in recent years, which is being threatened by the abuse of food additives, especially additive residues in animal tissue. Ractopamine (Rac) is an artificially synthesized betaagonist that belongs to the phenolic group [39]. Nowadays, Rac is widely used as feed additive in some animal species such as swine, cattle and turkeys [39]. Although the application of Rac can improve the production of muscle tissues via diverting nutrients from fat to deposition [40-41], there still exists a potential danger for consumer health because it readily accumulates in animal tissues [42]. Based on this fact, there is an urgent need for a sensitive and accurate method for the determination of Rac residues in animal tissues. Up-to-now most of the analytical methods towards these determinations require a well-equipped laboratory, trained personnel, high capital expenditure and involve time-consuming sample preparation steps. These added to the cost and complexity of assay. Consequently, the development of a convenient, rapid, accurate, simple and economy analytical method for the determination of these food contaminants is highly desirable. Interestingly, so far Fe₃O₄/rGO nanocomposite has not been developed for the electrocatalytic detection of these food contaminants.

7. Objectives

1. To construct and develop a disposable food contaminant sensor based on a screen-printed electrode modified with Fe₃O₄/rGO nanocomposites.

- 2. To connect the excellent physicochemical properties of rGo with magnetism and biocompatibility of Fe_3O_4 nanoparticle through simple and facile chemical method and explore their application towards fabrication of a glucose/ O_2 enzymatic biofuel cell
- 3. To improve system enzyme immobilization, electron transfer efficiency, electrical power density, stability, extended life time with nanocomposite including Fe₃O₄ magnetic nanoparticels and reduced graphene oxide

8. Methodology

1. Preparation of Fe₃O₄/rGO nanocomposite modified electrode

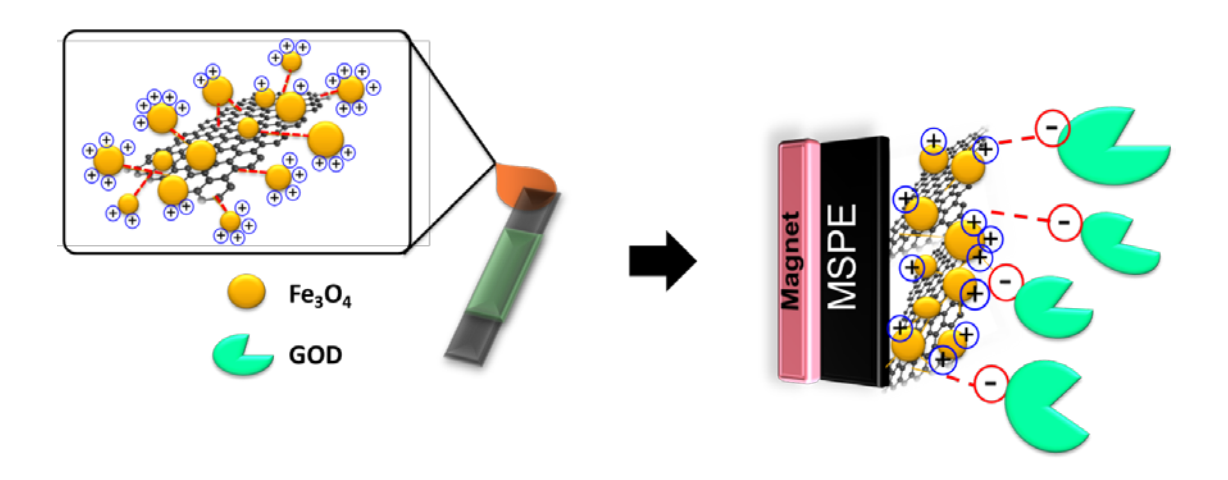
The NH₂-Fe₃O₄ NPs were prepared through a solvothermal reaction according to F. Zhang et al. 2011 [43]. The Fe₃O₄ NPs was immobilized on GO using EDC and NHS as coupling agents by the formation of an amide link between the amino group of Fe₃O₄ NPs and the carboxyl group of GO. 20 mg GO in 60 mL water was ultrasonicated for 3 h, and then 100 mg EDC and 80 mg NHS were added into the solution of GO. The mixture was stirred for 30 min and ultrasonicated for another 30 min to form a homogenous suspension. Next, 20 mg of NH₂-Fe₃O₄ NPs was added into the suspension solution and the mixture was subjected to ultrasonication for 30 min. The reaction was carried out at 80 °C for 1 h under stirring. The Fe₃O₄/rGOnanocomposite was obtained by magnetic separation and washed with water several times.

An Fe₃O₄/rGO nanocomposite based on glucose reduction was prepared. In brief, 40 mg glucose was added into a 25 mL Fe₃O₄/rGO dispersion solution followed by stirring for more than 0.5 h. and 20 μ l ammonia solution (25% w/w) was added into the resulting dispersion solution. After being stirred for a few minutes, the mixture was again stirred for 60 min at 95 °C. Finally, the resulting stable black dispersion solution was centrifuged and washed with water several times. The obtained Fe₃O₄/rGO nanocomposite (1 mg/2.5 mL) was redispersed in DI water before further use. Finally, the 5 μ l Fe₃O₄/rGO nanocomposite solution was dropped onto the MSPCE surface.

2. Preparation of Fe₃O₄/rGO/GOD nanocomposite modified electrode

GOD was immobilized onto the Fe $_3$ O $_4$ /rGO nanocomposite modified MSPE through an electrostatic interaction between positive charges of Fe $_3$ O $_4$ and negative charges of GOD. 30 mg GOD was added into 1 mL 0.1 M PBS pH 7.0 solution. The Fe $_3$ O $_4$ /rGO nanocomposite modified MSPCE was immersed into the GOD solution (30 mg/mL in 0.1 M PBS pH 7.0), and then reacted at room temperature for 12 h. The

 ${\rm Fe_3O_4/rGO/GOD}$ nanocomposite modified electrode surface was washed with DI water to remove unadsorbed enzyme molecules and allowed to dry at room temperature. The modified electrode was stored at 4 °C when not in use. The fabrication process is shown in Scheme 1



Scheme 1. Schematic illustration of Fe₃O₄/rGO/GOD modified MSPCE

3. Magnetic screen-printed electrode fabrication

The magnetic screen-printed electrode (MSPCE) was prepared by a rectangular magnet sticker (1.5×2 mm) put onto the backside of a screen-printed electrode (SPCE).

4. Magnetic glassy carbon electrode fabrication

The magnetic glassy carbon electrode (MGCE) was prepared by placing a nummular NdFeB magnet (3 mm in diameter and 4 mm in thickness) on a glassy carbon (3 mm in diameter and 3 mm in thickness). A copper wire was put around the magnet and filled with silver glue, which was then put into an acrylic tube (10 mm in diameter and 20 mm in depth). All components were fixed with epoxy resin then cured at room temperature for at least 24 h. The MGCE was successively polished with emery paper and alumina powder, followed by sonication in DI water.

5. Bioelectrode fabrication

GOD was immobilized onto the Fe_3O_4/rGO modified MGCE through electrostatic interaction between the positive charge of Fe_3O_4 and the negative charge of GOD. 30 mg of GOD was added into 1 mL 0.1 M PBS pH 7.0 solutions. The Fe_3O_4/rGO modified MGCE

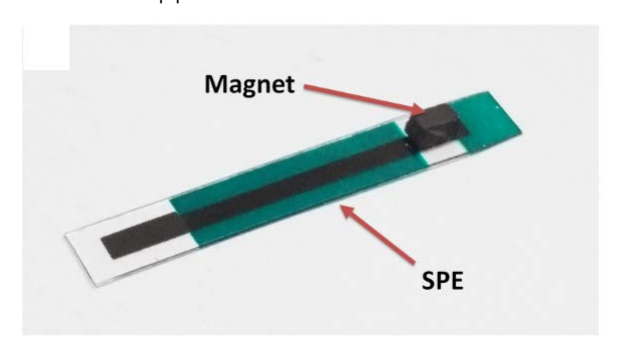
was immersed into the GOD solution (30 mg/mL in 0.1 M PBS pH 7.0) then reacted at room temperature for 24 h. The $Fe_3O_4/rGO/GOD$ modified surface was washed with DI water to remove the unadsorbed enzyme molecules and allowed to dry at room temperature. The modified electrode was stored at 4 °C when not used. The preparation of biocathode used BOD instead of GOD.

6. Biofuel cell set up

The EBC cell constructed with three-dimensional printer (3D printer) using poly(lactic acid), PLA as a material. The EBC cell consists of Fe₃O₄/ rGO/ GOD and Fe₃O₄/rGO/BOD as bioanode and biocathode, respectively, with electrode spacing of 0.5 cm. The EBC system was fed with 0.1 M PBS pH 7.0 containing 5 mM of glucose delivered to the electrode chamber using a peristatic pump. The voltage output was measured using a multi-meter with application of external resistance ($R_{\rm ext}$) varying from 10 M Ω to 200 Ω . The voltage was used to calculated power (P) according to the equation P=IV/A, where I is the current, V is the voltage and A is the area of the electrode. The EBC was operated at human physiological temperature (37 ± 1 °C).

7. Preparation of the sensor for ractopamine determination

The screen-printed electrodes (SPCE) used in this study were obtained from Quasense Co., Ltd. (Thailand). The MSPCE was prepared by a rectangular magnet sticker (1.5 x 2 mm) put onto the backside of SPCE. To prepare the sensor, 5 μ L of Fe₃O₄/rGO nanocomposite solution was dropped on the surface of MSPCE and dried in air.



8. Preparation of real samples

Different samples of pork and liver were purchased from a local supermarket and then treated as follows. Firstly, 2 g of smashed peeling, grinding sample was added into 10 mL 0.1 M HClO₄. After being homogenized for 20 min, and heated at 80°C for 30 min, the vial was put in the water bath and centrifuged. After that, the clear liquid phase was

สัญญาเลขที่ RSA5980073

collected and then $10\%~Na_2CO_3$ and then 1.6~g~NaCl was slowly added to adjust the pH value of the collected liquid to 10. Subsequently, RAC was extracted twice using 5~mL ethyl acetate. Lastly, RAC was reverse extracted to 2~mL with 0.1~M HCl solution. The reverse extraction was repeated, and the above extracted solution was diluted with 0.1~M PBS pH7.0 to 10~mL. Spiked samples were prepared in the same step; a known amount of RAC standard was added to the sample before treatment.

Results and Discussion

1. Characterization of Fe₃O₄/rGO/GOD nanocomposite

The surface morphology of GO characterized by SEM is shown in Fig. 1a. A few layers of GO sheets appear partially packed with their basal planes, intensely crumpled and folded into a typical wrinkled structure. These geometric wrinkling and rippling were caused by nanoscale interlocking of GO sheets. The spherical Fe₃O₄ NPs were clearly observed as shown in Fig. 1b and distributed well on the whole surface of a rGO sheet due to the strong interaction of covalent bond (Fig. 1c). The diameter of Fe₃O₄ NPs was about 32 nm. In Fig. 1d, after the immobilization of GOD on the Fe₃O₄/ rGO nanocomposite by electrostatic force, the nanocomposite showed deposition of a protein globular structure on the uniform structure and the roughness increased dramatically indicating that the enzymes were successfully immobilized on the surface of the Fe₃O₄ NPs and the size of particles was slightly increased. The results confirm the preparation of the nanocomposite.

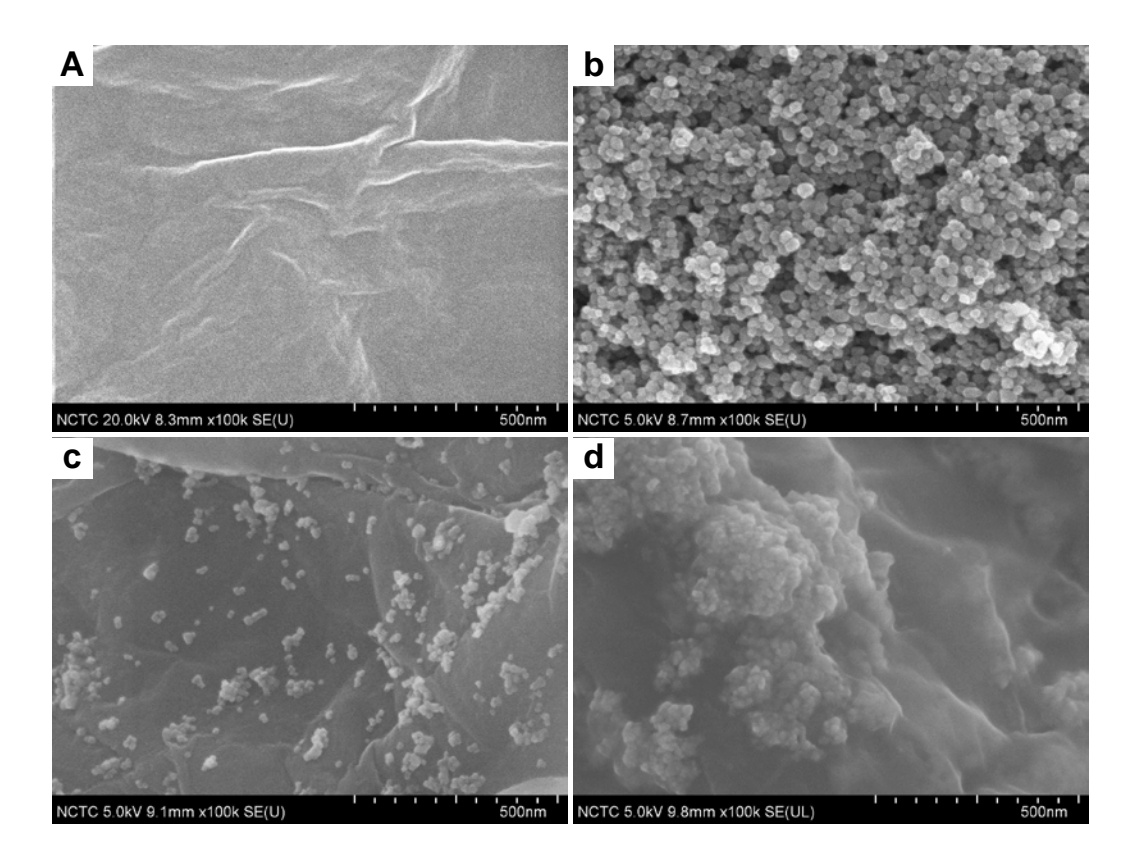


Fig. 1. SEM images of (a) GO, (b) Fe $_3$ O $_4$ NPs, (c) Fe $_3$ O $_4$ /rGO nanocomposite and (d) Fe $_3$ O $_4$ /rGO/GOD nanocomposite.

2. Fourier transform infrared (FT-IR) study of Fe₃O₄/rGO nanocomposite

The Fe₃O_a/ GO nanocomposite was obtained from the NHS and EDC and the condensation reaction between the amino group of Fe₃O₄ NPs and carboxylic group of GO which formed a carboxamide bonding. The confirmation of binding between the GO and Fe₃O₄ NPs was studied by FT-IR spectroscopy. The FT-IR spectra of the NH₂-Fe₃O₄ NPs (curve a), GO (curve b), and Fe₃O₄/GO nanocomposite (curve c) are shown in Fig. 2A. The band of NH₂-Fe₃O₄ NPs, as shown in curve a, was found at 571 cm⁻¹, which corresponded to the Fe-O stretching vibration, and the two spectrum bands observed at 1630 and 3351 cm⁻¹ were assigned to the N-H bending and stretching vibrations of free amino groups on the Fe₃O₄ NPs as reported [44]. The results indicated that the amino group has been grafted onto the Fe₃O₄ NPs surface. Fig. 2A curve b shows the FT-IR spectrum of GO, and a strong and broad absorption at 3401 cm⁻¹ was observed, which was due to the O-H stretching vibration. The absorptions' peak at 1724 and 1375 cm⁻¹ corresponded to the C=O stretching of carboxylic acid and carbonyl moieties. For the aromatic C=C and the epoxy group, alkoxy C-O, stretching vibrations were observed at 1625 and 1084 cm⁻¹, respectively [45]. In curve c, after introducing the Fe₃O₄ NPs on GO, the FT-IR spectrum of the Fe₃O₄/GO appeared in the band at 565 cm⁻¹ and illustrated the Fe–O stretching vibration, confirming the deposition of Fe₃O₄ on GO. Three new characteristic peaks of the amide carbonyl group for Fe₃O₄/GO nanocomposite at 1634 (-CONH amide band I), 1544 (-NH amide band II), and 1368 cm⁻¹ (C-N stretch of amide) appeared, implying that Fe₃O₄ NPs were successfully linked to the GO sheet via covalent bonding after the amidation reaction [46]. The two bands at 3284 and 1634 cm⁻¹ were attributed to the O-H stretching vibration, and to the N-H stretching vibrations and the NH₂ bending mode of the free NH₂ group, respectively. However, the Fe₃O₄/ GO nanocomposite is still composed of functional groups with an oxygen component such as hydroxyl and ether groups on both sides. Glucose was applied as a reducing agent to remove oxygen components. The FT-IR spectra of Fe₃O₄/ GO nanocomposite and Fe₃O₄/rGO nanocomposite are presented in Fig. 2B, curves a and b, respectively. In the Fe₃O₄/GO spectrum, the graph shows the stretching of hydroxyl group at 3284 cm⁻¹(O−H stretching), the C=O carbonyl stretching at 1634 cm⁻¹ and 1718 cm⁻¹, as well as the C-O epoxide group stretching at 1060 cm⁻¹. All these bands related with the oxygencontaining functional groups mostly remain in the FT-IR spectrum of the Fe₃O₄/ GO nanocomposite. The high intensity of the main peaks in the Fe₃O₄/GO nanocomposite confirmed the presence of a large number of oxygen functional groups as shown in Fig. 2B curve a. After the GO was chemically reduced, the characteristic absorption bands of

hydroxyl at 3168 cm $^{-1}$ were significantly decreased. The carbonyl group at 1554 cm $^{-1}$ and 1368 cm $^{-1}$, and alkoxy groups at 1060 cm $^{-1}$ in curve b disappeared, indicating the high efficiency of reduction and oxygen-containing functional groups' removal from the GO. The absorption band that appears at 1629 cm $^{-1}$ may be attributed to the skeletal vibration of the graphene sheets [47]. Moreover, observing an additional peak can be ascribed to the lattice absorption of Fe $_3$ O $_4$ NPs at 572 cm $^{-1}$. These confirmed that most of the oxygen-containing functional groups were already removed.

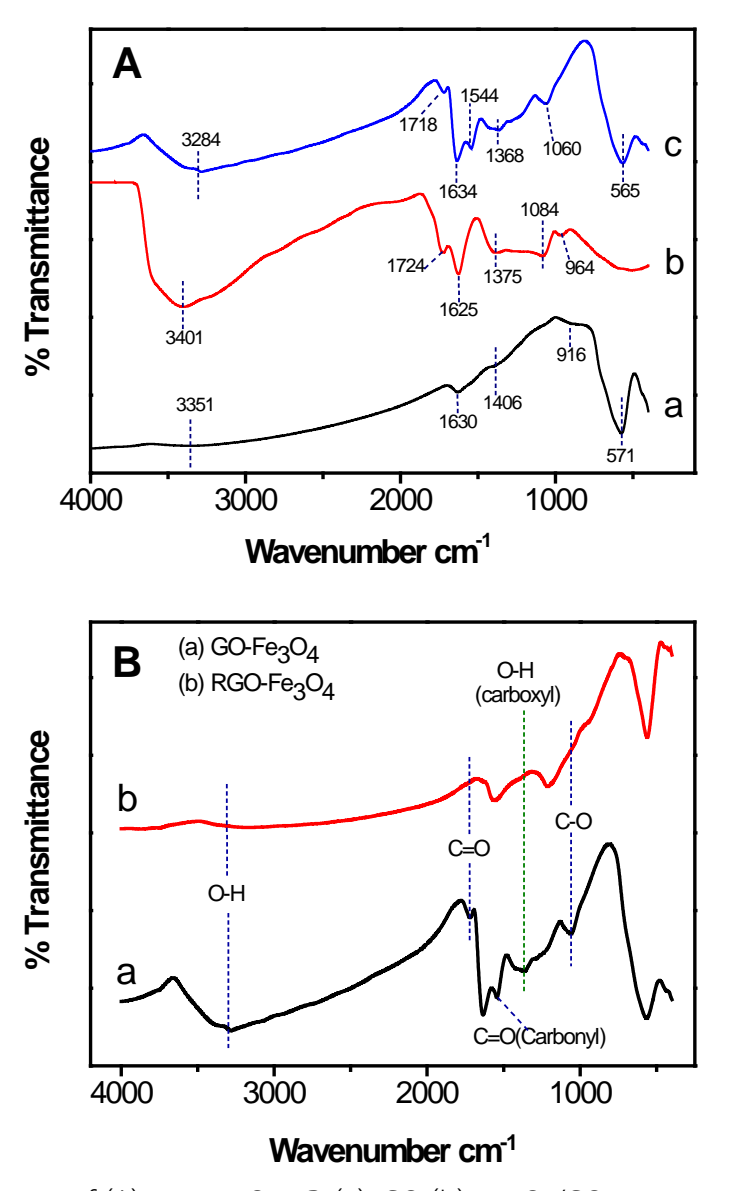


Fig. 2. FT-IR spectra of (A) NH_2 -Fe $_3O_4$ NPs(a), GO (b), Fe $_3O_4$ /GO nanocomposite (c), (B) FT-IR spectra of Fe $_3O_4$ /GO nanocomposite (a) and Fe $_3O_4$ /rGO nanocomposite (b).

3. Raman spectroscopy study of Fe₃O₄/rGO nanocomposite

Raman spectroscopy was used to investigate the electronic structure of graphene and characterize the reduction degree of the GO. The Raman spectroscopies of the GO, Fe₃O₄/GO and Fe₃O₄/rGO are shown in Fig. 3. Typically, the Raman spectrum of graphene was characterized by two fundamental vibrations the G band corresponds to the first order scattering of the E2g phonon of sp² C atoms (usually observed at \square 1575 cm⁻¹), a characteristic band of crystalline graphite, and the D band indicates the reduction in size of the in-plane sp² domains for the chemical oxidation of graphite (\square 1350 cm⁻¹) [47-48]. In the Raman spectrum of the GO (curve a), the G band is broadened and blue shifts to 1597 cm⁻¹, which is attributed to the presence of isolated double bonds that resonate at higher frequencies than the G band of graphite. The D band at 1358 cm⁻¹ becomes prominent, indicating the reduction in size of the in-plane sp² domains due to the extensive oxidation. As shown in Fig. 3 curve c, the Raman spectrum of the Fe₃O₄/rGO exhibits D and G at 1346 and 1594 cm⁻¹, and the G band of Fe₃O₄/rGO moves to 1594 cm⁻¹, which is closer to that of graphite, indicating the GO was reduced. The intensity ratio of the D to G peak (I_D/I_G) is found to change inversely with graphitic domain size and widely used to study the crystalline quality of graphite or graphene after the treatment. The I_D/I_G improved from the GO was 0.83, Fe₃O₄/GO (0.89) to Fe₃O₄/rGO (1.03). This change suggested that more sp² domains are formed during the reduction of graphite oxide. This increase is due to the decrease of the sp² in-plane domain induced by the introduction of defects and disorder of the sp² domain.

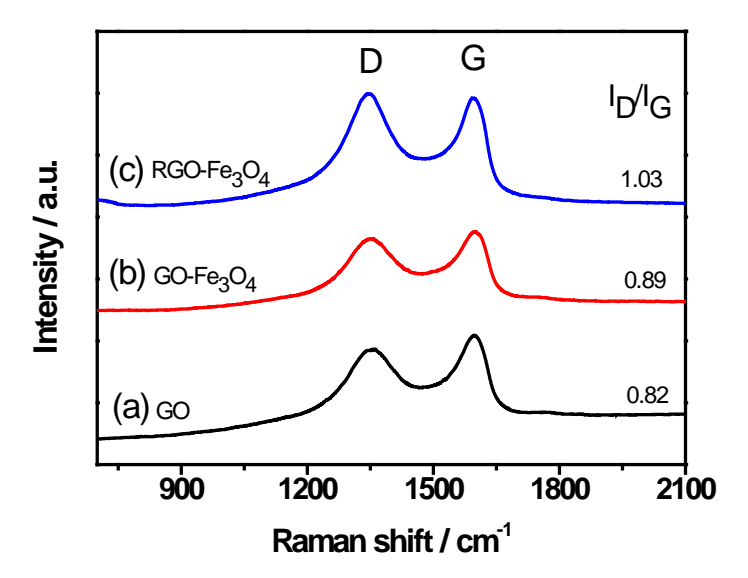


Fig. 3. Raman spectra of GO (a), Fe₃O₄/GO (b) and Fe₃O₄/rGO (c).

4. Direct electrochemistry of GOD immobilized Fe₃O₄/rGO modified electrode

The electrochemical properties of nanocomposite were studied using cyclic voltammetry. Under appropriate conditions, the DET between the GOD and the substrate can be observed from the electrochemical response. Fig. 4A shows the cyclic voltammograms of GOD-modified different electrodes in the N_2 -saturated PBS at a scan rate of 100 mV/s. No redox peaks were observed for the GOD-MSPCE (curve a) and Fe_3O_4/GOD -MSPCE (curve b). The background current of the Fe_3O_4/GOD -MSPCE was higher than that of the GOD-MSPCE, and is ascribed to the large surface area of the Fe_3O_4 , which showed a distinct electrochemical response.

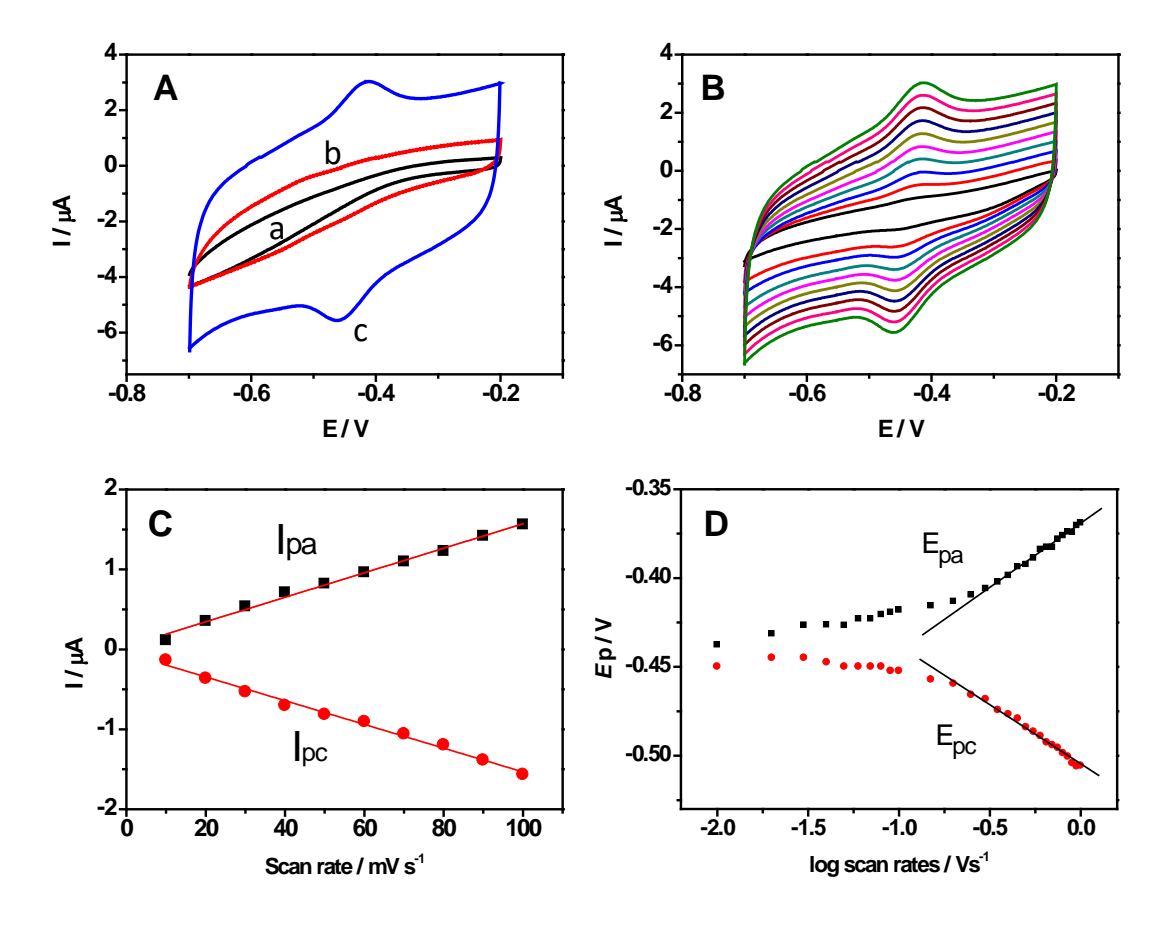


Fig. 4. (A) Cyclic voltammograms of the different modified electrodes with GOD-MSPCE (a), Fe₃O₄/GOD-MSPCE (b) and Fe₃O₄/rGO/GOD-MSPCE (c) in 0.1 M PBS pH 7.0 with N₂-saturated at a scan rate of 100 mV/s. (B) CVs of the Fe₃O₄/rGO/GOD-MSPCE in 0.1 M PBS pH 7.0 at different scan rates inner to outer: 10, 20, 30, 40, 50, 60, 70, 80 and 100 mV/s. (C) The relationship of the peak current (I_p) vs. the scan rates. (D) The relationship of the peak potential (E_p) vs. the logarithm of scan rates (log V).

Fig. 4A, curve c showed a well-defined redox peak with an anodic peak potential (E_{pa}) at -0.418 V and a cathodic peak potential (E_{pc}) at -0.452 V. The peak potential separation (ΔE_p) was about 34 mV. These results demonstrated a fast DET kinetics of the GOD on the surface of the Fe₃O₄ on the graphene sheet. The well-defined and quasi-reversible redox peaks suggested a favorable DET between the electrode and the redox centers of the GOD molecules. The formal potential (E^0) obtained by averaging the potential values of the E_{pa} and E_{pc} was -0.435 V. This value was close to the standard electrode potential of -0.483 (vs. Ag/AgCl) for FAD/FADH₂ at pH 7.0 [49], suggesting that the GOD molecules retain their bioactivity after the adsorption on the Fe₃O₄/rGO nanocomposite, and the electrochemistry response of the GOD immobilized on the modified electrode is due to the redox reaction of the FAD.

5. The influence of the scan rate

The effect of the scan rate on the cyclic voltammetric performance at the Fe₃O₄/rGO/GOD modified MSPCE with different scan rates is shown in Fig. 4B, where the redox processes of the nanocomposite gave mostly symmetric anodic and cathodic peaks (E_{pa} and E_{pc}) at relatively slow scan rates. When the scan rate increased, the redox potentials of the GOD shifted slightly. The anodic and cathodic peak currents (I_{pa} , I_{pc}) linearly increased with the increasing scan rate from 10 to 100 mV/s, indicating that the redox reaction of the GOD on the Fe₃O₄/rGO modified electrode was a quasi-reversible surface-controlled process. The plot of the cathodic peak current versus the scan rate showed a linear relationship (Fig. 4C) with linear regression equations: I_{pa} = 0.0153x+ 0.0383, I_{pc} = -0.0149x-0.0475 with a correlation coefficient (R²) of 0.993 and 0.992, respectively. These results demonstrated a fast DET kinetics of the GOD on the surface of the graphene.

According to Laviron's equation [50], the plots of the E_{pa} and E_{pc} versus the logarithm of the scan rates produced two straight lines with slopes of $2.3RT/(1-\alpha)nF$ and $-2.3RT/\alpha nF$ at high scan rates (up to 1000 mV/s) as shown in Fig. 4D. The charge transfer coefficient (α) and the heterogeneous electron transfer rate constant (k_s) for the proposed electrode were calculated to be 0.5 and 13.78 s⁻¹, respectively, according to the following equation:

$$\log k_s = \alpha \log(1-\alpha) + (1-\alpha)\log \alpha - \log \frac{RT}{nFv} - \frac{\alpha(1-\alpha)nF\Delta E_p}{2.3RT}$$
(1)

Where R is gas constant, T is temperature, v is scan rate and ΔE_p is peak separation. This result confirmed that the Fe₃O₄/rGO facilitated the fast electron transfer between the redox-active site of enzyme and the surface of the electrode. These results suggest that the Fe₃O₄/rGO/GOD provides fast electron transfer kinetics between the redox center of the enzyme and the surface of the electrode. The superior electron transfer kinetics of graphene can be ascribed to their unique electronic structures, which are favorable for conducting electrons from the redox center to the electrode surface. The surface average concentration of GOD (Γ , mol/cm²) on the electrode can be calculated from the charge integration of the cathodic peak in the cyclic voltammogram according to the formula, $\Gamma = Q/nFA$, where Q is the charge consumed in C, n is the number of electrons transferred (n= 2 for DET of GOD), A is the electrode area (cm²) and F is the faraday constant. The electroactive GOD concentration on the Fe₃O₄/rGO was estimated to be 4.95×10^{-11} mol/cm², indicating a saturated adsorption of the GOD the on Fe₃O₄ surface of the nanocomposite which is higher than previously reported at a GOD on a mesoporous iron oxide modified SPCE [41].

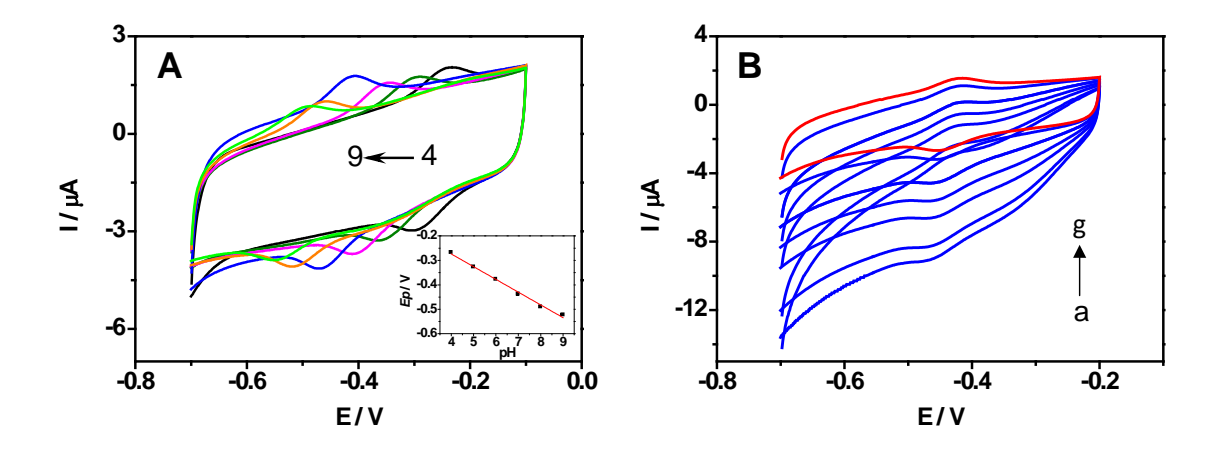


Fig. 5. (A) CVs of the Fe₃O₄/rGO/GOD-MSPE in 0.1 M PBS with different pH values of 4, 5, 6, 7, 8 and 9 at a scan rate of 50 mV/s. (B) CVs of Fe₃O₄/Rgo/GOD-MSPE in 0.1 M PBS pH 7.0 at a scan rate of 30 mV/s in the presence of various concentrations of glucose (a) O₂-saturated without glucose and with glucose concentration of 0.5 (b), 1 (c), 4 (d), 8 (e) and 10 mM (f) and N₂-saturated without glucose (g).

6. The influence of solution pH

It is well known that the direct electrochemistry of a GOD has a two-electron coupled with two-proton reaction. Therefore, the pH value of the solution should have

an effect on the electrochemical behavior of the GOD on the Fe₃O₄/rGO , and a negative shift of both the cathodic and anodic peak potentials occurs when the solution's pH value was increased as shown in Fig. 5A. The redox potential $E^{0'}$ changes linearly as a function of the solution pH from 4 to 9 with a slope of –52 mV/pH (r^2 = 0.9989). This slope is close to the theoretical value of –58.6 mV/Ph [52] according to the reaction of equation (2) for a reversible reaction, indicating two protons (2H⁺) and two electrons (2e⁻) attending in the electron transfer process. The reaction mechanism can be written as follows:

$$GOD (FAD) + 2e^{-} + 2H^{+} \longleftrightarrow GOD (FADH_{2})$$
 (2)

7. Electrocatalytic activity of the Fe₃O₄/rGO/GOD-MSPCE to glucose

In order to study the enzymatic catalytic activity of the GOD adsorbed on the Fe3O4/rGO -MSPCE, the experiments were carried out by cyclic voltammetry. Fig. 5B shows the CVs of the Fe3O4/rGO/GOD-MSPCE with different glucose concentration in 0.1 M PBS pH 7.0 at the scan rate of 30 mV s⁻¹. Under N₂-saturated condition (curve g), a pair of well-defined and almost symmetrical redox peaks was observed, which indicates that a GOD adsorbed on an Fe3O4/ rGO-MSPCE can undergo a reversible direct electrochemical reaction, and this implies the DET of the GOD for FADH2 oxidation and FAD reduction in equation (2). In O₂-saturated condition (curve a), the reduction peak current of the Fe₃O₄/rGO/GOD-MSPCE was larger than that in the N₂-saturated PBS and the oxidation peak current was smaller. The reason for this is that the GOD (FADH₂) was oxidized to regenerate the oxidized form of the GOD (FAD) because O2 is a natural cosubstrate for the GOD. It confirms that oxygen dissolved in the PBS solution was reduced at the electrode according to the following equations (3) which was a typical electrochemical catalytic process, in which oxygen regenerates the GOD (FAD) and enhances the reduction peak current of the FAD. When glucose was added into this system (curve b-f), the GOD reacted with the glucose and turned FAD into the reduced form of the GOD (FADH₂) as shown in equation (4). Fig. 5B, curve b-f shows the CVs of the Fe₃O₄/rGO/GOD-MSPCE with various concentrations of glucose. It was found that the reduction peak currents decrease with increasing glucose concentration ranging from 0.05 mM to 10 mM due to the enzyme-catalyzed reaction that occurred and the decrease of the FAD form concentration at the electrode surface, indicating that the GOD retains its high bioelectrocatalytic activity to the glucose. The results were consistent with the previous reports [53]. Therefore, based on the decrease of the reduction current, the concentration of glucose can be detected and used as a biosensor system for reagentless glucose sensing. The electrocatalytic mechanism can be expressed as follows:

$$GOD (FADH2) + O2 \longrightarrow GOD (FAD) + H2O2$$
 (3)

$$GOD (FAD) + Glucose \rightarrow GOD (FADH_2) + Gluconolactone$$
 (4)

8. Amperometric response of the glucose biosensor

From the relationship between the decrease of the reduction current and the concentration of glucose, the amperometry technique was used to perform at the applied potential of -0.45 V in 0.1 M PBS pH 7.0. Fig. 6A shows typical steady-state amperometric responses of the Fe₃O₄/rGO/GOD-MSPCE on successive injections of glucose under stirring. The steady-state current obtained on the Fe₃O₄/rGO/GOD-MSPCE decreased during the addition of glucose concentration. The electrocatalytic response was very fast as the biosensor achieved the maximum response after 3 s when glucose was added into the solution. As the inset of Fig 6A, the resulting calibration plot is presented over the concentration range 0.05 to 1.2 mM. It was found that the reduction current response decreased with increasing proportional to the glucose concentration. The plot of current response vs. glucose concentration was linear in the ranges of 0.05 to 1 mM with the linear regression equation of y = 5.873x + 0.131 (correlation coefficient 0.993) and a sensitivity of 5.9 μ A/mM. The detection limit was calculated to be 0.1 μ M at a signal-to-noise ratio of 3 (S/N=3).

The comparison of the analytical performance of the developed electrode with some other previous reports on direct glucose biosensors are summarized in Table 1. It can be seen that this biosensor exhibits a lower detection limit and a higher sensitivity compared with other Fe₃O₄ electrodes and SPCE based glucose biosensors. Typically, the DET was extremely difficult to occur at SPCE more than at GCE because of the lower sensitivity and surface area. The presence of the Fe₃O₄ and graphene could increase the conductivity of the electrode and the GOD could quickly transfer electrons to electrodes. The resulting good performance was not only due to the strong bonding but the paramagnetism force might reduce the spacing of enzymes and increase the amount of nanocomposites to entrap into the porous SPCE surface.

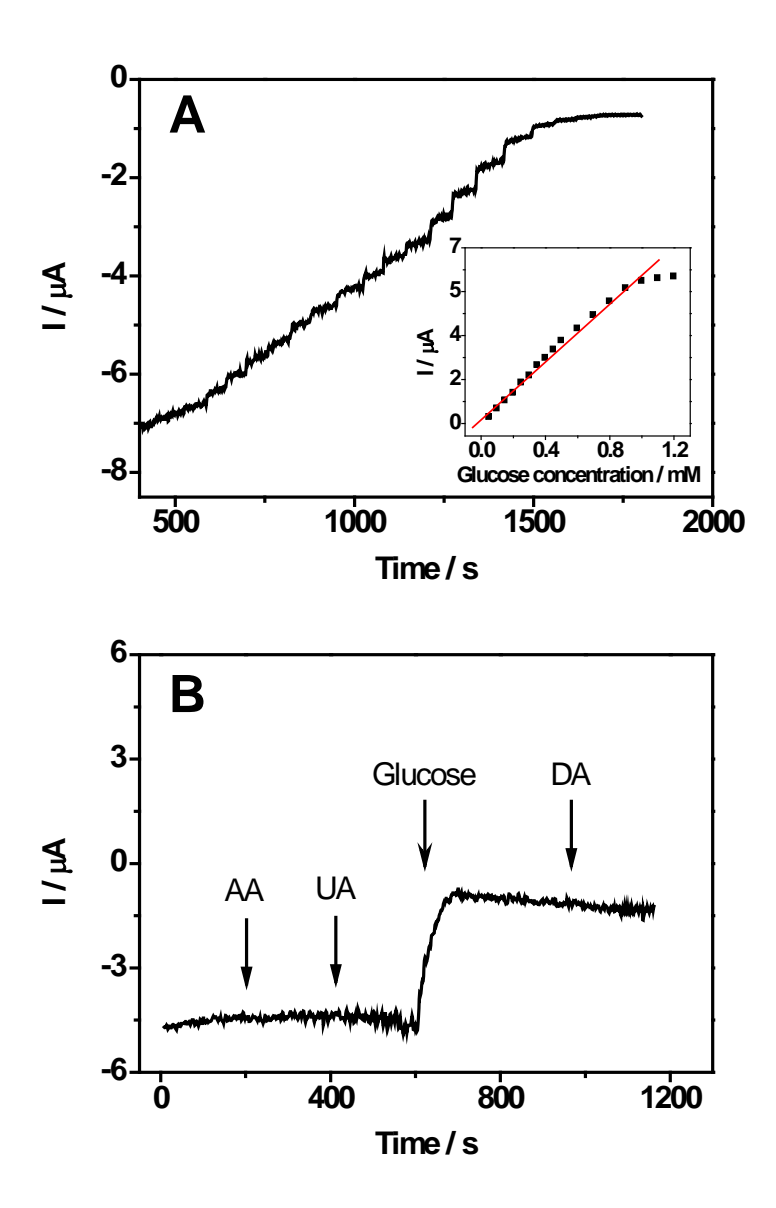


Fig. 6. Amperometric response of (A) Fe $_3$ O $_4$ /rGO/GOD-MSPCE to successive addition of glucose concentration at applied potential of -0.45 V in 0.1 M PBS pH 7.0. Inset is the calibration curve for glucose obtained at the biosensor. (B) Fe $_3$ O $_4$ /rGO/GOD-MSPCE to 1 mM UA, 1 mM AA, 0.5 mM glucose and 1 mM DA at the applied potential of -0.45 V in 0.1 M PBS pH 7.0.

The apparent Michaelis-Menten constant (K_M^{app}) values were evaluated by an electrochemical Lineweaver-Burk equation [54-55] which can provide an indication of the enzyme–substrate kinetics.

$$\frac{1}{I_{ss}} = \frac{1}{I_{\text{max}}} + \frac{K_M^{app}}{I_{ss}} \cdot \frac{1}{C} \tag{5}$$

Here, $I_{\rm ss}$ is the steady-state current, C the concentration of substrate, and $I_{\rm max}$ the maximum current response. The corresponding plot yielded an "apparent" $K_{\rm m}$ of 0.16 mM. The value was smaller than those reported for the DET of the GOD [56-59] indicating that it has a higher affinity towards glucose. The good microenvironment due to the synergistic effect of the nanocomposite might contribute to the improvement of the affinity and good performances of the biosensor.

Table 1 Comparison of analytical performance of DET glucose biosensors based Fe_3O_4 and SPCE.

Modified electrodes	$k_{\rm s}({\rm s}^{-1})$	Linear range (mmol l ⁻¹)	LOD (µ mol l ⁻¹)	Immobilized method	K _m (mM)	Ref.
Silica sol-gel/PVA/SPE	8.38	0 - 4.13	9.8	Sol-gel	-	[60]
Nafion/preanodized SPE	4.38	0.1 - 0.9	-	Polymer	1.07	[57]
				entrapment		
Fe ₃ O ₄ -AuNPs-CS/AuE	-	0.003 - 0.57	1.2	Polymer	-	[61]
				entrapment		
Aunps-PDA-Fe ₃ O ₄ -MGCE	3.8	0.02 - 1.875	6.5	Polymer	1.67	[58]
				entrapment		
GNs/ZnO/SPE	3.75	0.3 - 4.5	70	Physical	-	[62]
				Absorption		
RGO-Fe ₃ O ₄ -MGCE	3.4	0.05 - 1.5	0.15	Physical	0.34	[59]
				Absorption		
Fe ₃ O ₄ /rGO-MSPE	13.78	0.05 - 1	0.1	Covalent,	0.16	This
				electrostatic		work

RGO: reduced graphene oxide, GCE: glassy carbon electrode, PVA: polyvinyl alcohol, AuNPs: gold nanoparticles, PDA: poly (dopamine), MGCE: magnetic glassy carbon electrode, GNs: graphite nanosheets, ZnO: zinc oxide nanoparticles, AuE: gold electrode, CS: chitosan

9. Repeatability and stability of the Fe₃O₄/rGO/GOD-MSPCE

The reproducibility of the biosensor was investigated by the amperometric method. The relative standard deviation (RSD) was calculated to be 3.98%, which was determined by 5 different modified electrodes of 0.5 mM glucose. The result demonstrates that the reproducibility and precision of the sensor was good. The stability was tested by measuring the decrease in the cyclic voltammetric current during potential cycling in 0.1 M PBS pH 7.0. The peak height and peak potential of the immobilized enzyme on Fe₃O₄/rGO remained nearly unchanged and the amount of the GOD remaining on the electrode surface was almost 98.4% of its initial value after 50 cycles. Furthermore, the long term stability of the biosensor exhibited a current response that retention of 95.6% after being stored at 4°C for 1 month which indicated that the nanocomposite modified electrode had high long term stability due to the strong covalent attachment of Fe₃O₄/rGO and electrostatic attraction of GOD onto the electrode surface, preventing enzymes from leaking out of the electrode surface.

10. Interference study

Common interference in blood such as ascorbic acid (AA), uric acid (UA), and dopamine (DA) usually coexist with glucose in human blood, which can interfere with the current signal. The direct electrochemistry of the GOD could avoid the interferences in the procedure of detecting glucose. The normal physiological level of glucose is 3 to 8 mM, which is much higher than those of the interfering species of AA (~ 0.1 mM) and UA (~ 0.02 mM). The amperometric current responses of the Fe₃O₄/rGO/GOD-MSPCE to the addition of 0.1 mM UA, 1 mM AA, 1 mM DA and 0.5 mM glucose at the applied potentials of -0.45 V in 0.1 M PBS pH 7.0 were evaluated. As can be seen in Fig. 6B, the interference was not observed. It can prove the selectivity of this biosensor.

11. Bioelectrode fabrication

The bioelectrodes fabrication was shown as schematic in Fig. 7. Due to Fe $_3$ O $_4$ NPs being surrounded by a positive charge, they play an important role in immobilizing enzymes through electrostatic interaction. GOD is a negatively charged biomolecule at pH 7.0 that can be easily immobilized onto the positively charged amino group on Fe $_3$ O $_4$ NPs surface via electrostatic interaction.

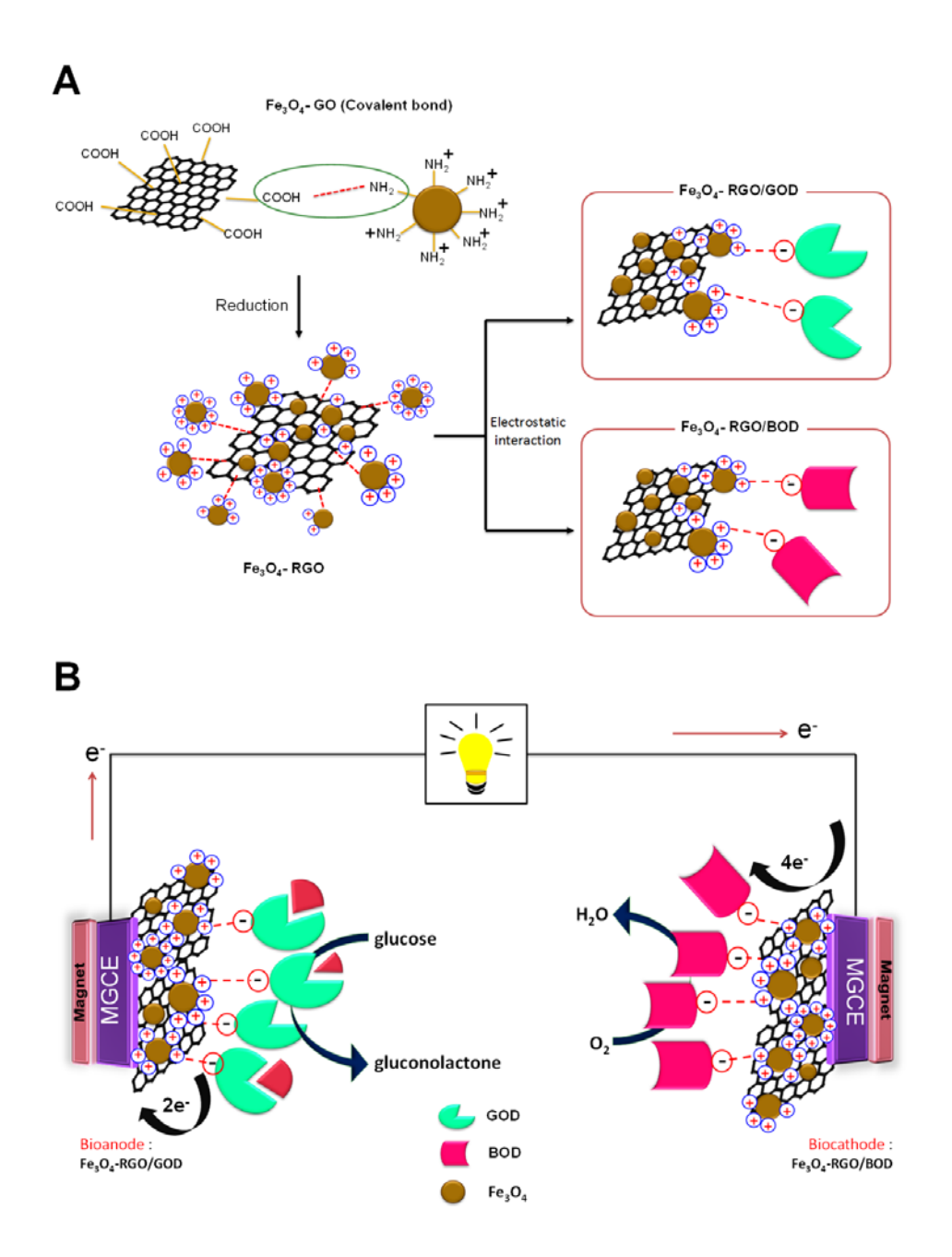


Fig. 7. Schematic representation of (A) the preaparation of Fe_3O_4 -/rGO and (B) the fabricated bioelectrodes for glucose EBC.

12. Electrochemical behavior of magnetic glassy carbon electrode (MGCE)

The electrochemical behavior of fabricated magnetic glassy carbon electrode (MGCE) was characterized by cyclic voltammetry. Ferricyanide ($K_3Fe(CN)_6$) was used as a redox probe to investigate the electrochemical behaviors of MGCE comparing to the bare

commercial glassy carbon electrode (GCE) with equal diameter of 3 mm at the scan rate of 50 mV/s in 0.1 M PBS pH 7.0. Fig. 8A, the CVs curve of the bare GCE in curve a showed a pair of well-defined quasi-reversible peaks with slightly lower peak current and larger peak separation potential than MGCE in curve b. Compared to the bare GCE, the redox peak currents of the bare MGCE increased greatly, implying that the MGCE electrochemical property can be applied for biosensors and BFCs.

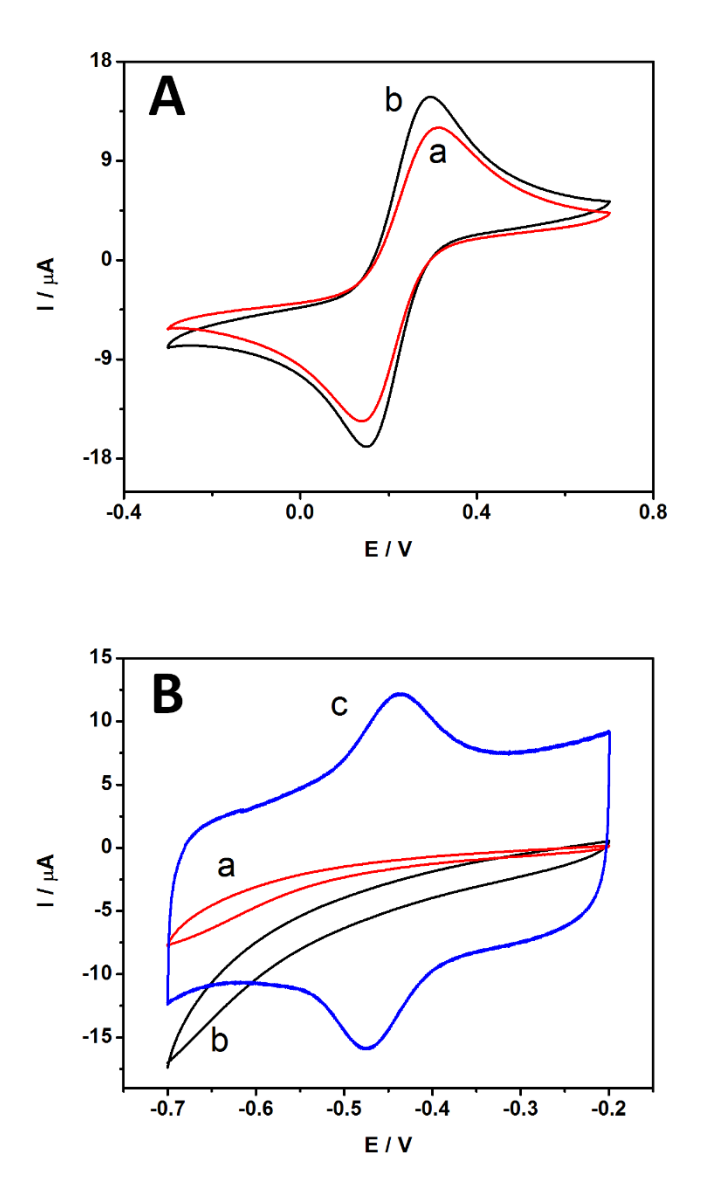


Fig 8. (A) Cyclic voltammograms (CVs) of bare GCE (a) and bare MGCE (b) in 0.1 M PBS pH 7.0 containing 2 mM $K_3Fe(CN)_6$ at a scan rate of 50 mV/s. (B) CVs of the different modified electrode with GOD-MGCE (a), Fe_3O_4/GOD -MGCE (b) and $Fe_3O_4/rGO/GOD$ -MGCE (c) in 0.1 M PBS pH 7.0 under N_2 -saturated at a scan rate of 100 mV/s.

13. Direct electrochemistry of GOD immobilized Fe₃O₄/rGO modified electrode

GOD molecules have flavin adenine dinucleotide (FAD) as redox centers deep localization inside the protein structure, thus the DET for GOD is extremely difficult. In order to improve the electron transfer of FAD, Fe₃O₄/rGO was applied to immobilize GOD. Fig. 8B shows the cyclic voltammograms of bare MGCE in N₂-saturated PBS at a scan rate of 100 mV/s. No peaks were observed for GOD-MGCE (curve a) and Fe₃O₄/GOD-MGCE (curve b). The background current of Fe₃O₄/GOD-MGCE was higher than the GOD-MGCE, which can be ascribed to the large surface area of Fe₃O₄ showing a distinct electrochemical response. In Fig. 8B, curve c shows redox peak of Fe₃O₄/rGO/GOD-MGCE with anodic peak potential (E_{po}) at -0.438 V and cathodic peak potential (E_{pc}) at -0.475 V. The peak potential separation (ΔE_p) is about 37 mV. These results demonstrate the fast DET kinetics of the GOD on the surface of Fe₃O₄ on the graphene sheet. The welldefined and quasi-reversible redox peaks suggest favorable direct-electron transfer between the electrode and redox centers of GOD molecules. The formal potential (E^0) obtained by averaging potential values of the E_{pa} and E_{pc} , was -0.457 V. This value is close to the standard electrode potential of -0.483 (vs. Ag/AgCl) for FAD/FADH2 at pH 7.0, suggesting that the GOD molecules retain bioactivity after adsorption on the Fe₃O₄/rGO nanocomposites. The DET process mechanism was described as GOD is two protons and two electrons coupled reaction, FAD serves as the catalytic site of GOD by accepting the electrons donated by the glucose and being reduced to FADH2. In this process glucose is converting into gluconolactone. (GOD)FADH2 is then oxidized by electrode to (GOD)FAD. Two protons and two electrons can subsequently be transferred from GOD to bioanode. O_2 is a natural electron acceptor for GOD. In presence of O_2 , GOD can be transfer electron to O₂ then reduced into hydrogen peroxide. Therefore, O₂ is a competing electron acceptor to DET reaction. Unfortunately, it is well know that DET system did not require oxygen due to FAD serves as the catalytic site of GOD by accepting the electrons donated by the glucose and being reduced to FADH2. The electrons can be transferred directly from GOD to electrode through Fe₃O₄/rGO composite. Moreover, based on membraneless EBC, the cathode compartment could be consumed most of O₂ for reduction reaction. In addition, the stability of Fe₃O₄/GOD-MGCE was also evaluated. There was no obvious change in redox peaks could be seen from the CV curves, the CVs curves still almost remained from their initial cycle after continuous scanning for 100 scan cycles. This can be implied that the fabricated electrode is very stable.

14. Electrocatalytic behavior of the Fe₃O₄/rGO/GOD-MGCE

Fig. 9 shows the CVs of the $Fe_3O_4/rGO/GOD-MGCE$ in a solution containing different concentrations of glucose under the condition of oxygen saturation. It can be seen from this figure that the reduction decreased with an increase in glucose concentration ranging from 0.5 mM to 8 mM. It can be explained that glucose is the substrate of GOD. When added to the air-saturated PBS, the enzyme-catalyzed reaction occurs and the concentration of the oxidized form of GOD present as GOD(FAD) at electrode decreases. Thus, the addition of glucose restrained the electrocatalytic reaction and led to the decrease of the reduction current. Therefore, this nanocomposite can serve as an efficient glucose sensor and EBC.

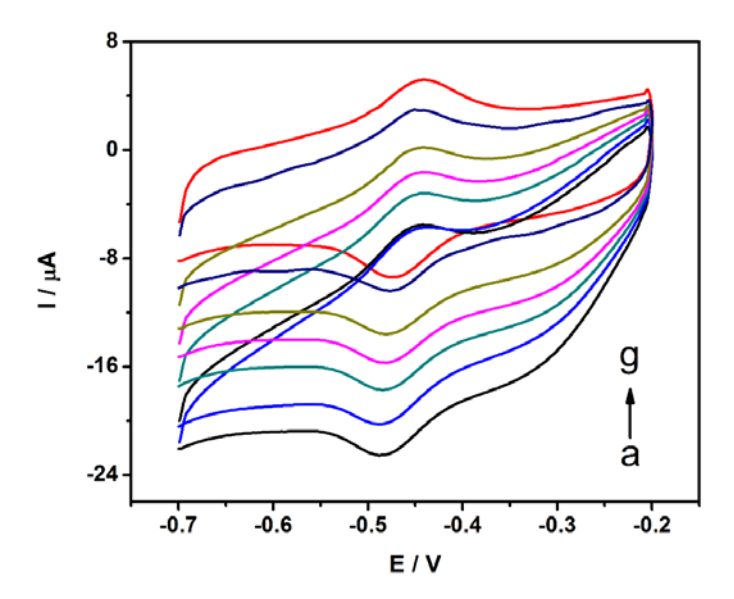


Fig. 9. CVs of Fe₃O₄/rGO/GOD-MGCE in 0.1 M PBS pH 7.0 at a scan rate of 50 mV/s in the presence of different concentrations of glucose O₂-saturated without glucose (a), with glucose concentration of 0.5, 1, 2, 4 and 8 mM (b-f) and N₂-saturated without glucose (g).

15. Electrocatalytic behavior of biocathodes

For biocathodes, the reduction of O_2 generally utilized two types of enzymes, including bilirubin oxidase and laccase. Laccase presents an optimum activity around pH 4-5. BOD electrocatalytic activity was investigated at neutral pH or pH 7.0 which was suitable for a real application system. BOD is one of the multicopper oxidase selected for catalyzing the four-electron reduction of oxygen to water at the biocathode because BOD can efficiently work as an electrode biocatalyst even under neutral conditions. In their structure, the T1 copper site gives electrons to the electrode and transfers those

electrons to the T2/T3 copper site, where oxygen is reduced to water in a four-electron transfer mechanism according to Equation 6. The electrocatalytic reaction of BOD on Fe_3O_4/rGO -MGCE as biocathode was examined using CV. The experiments were carried out under nitrogen saturated and oxygen saturated conditions at the potential between -0.4 V to + 0.8 V at a scan rate of 1 mV/s.

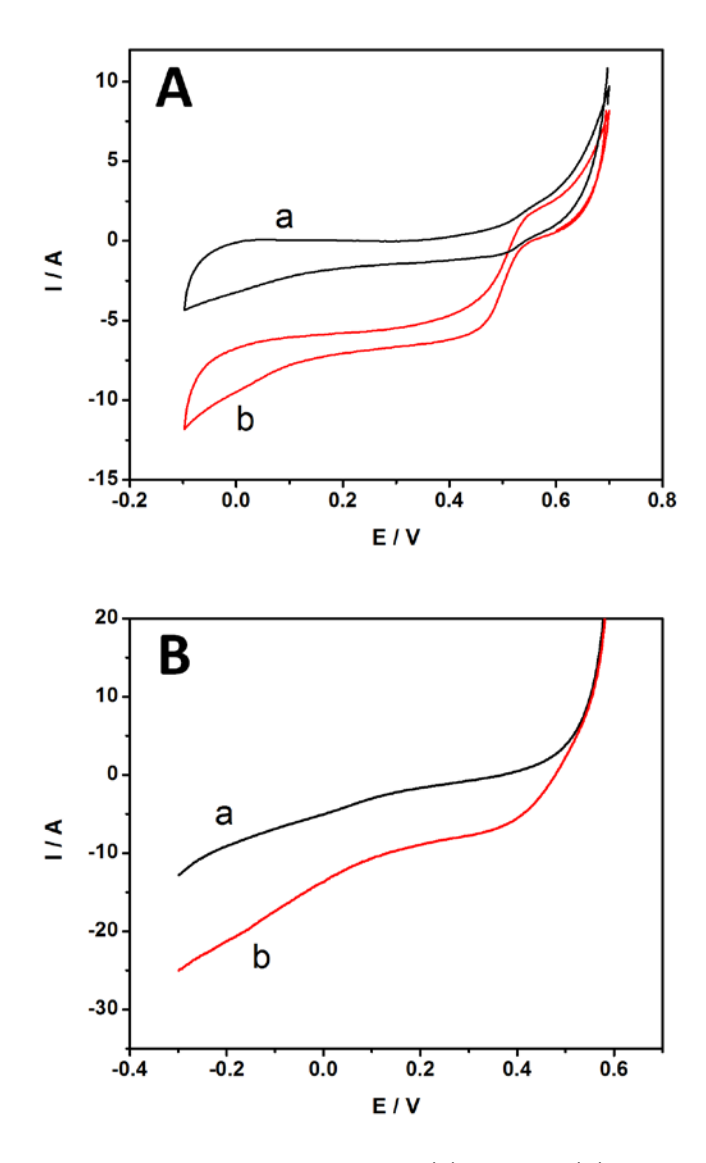


Fig. 10. (A) CVs of Fe₃O₄/rGO/BOD-MGCE under N₂ (a), and O₂ (b) saturated 0.1 M PBS pH 7.0 at a scan rate of 1 mV/s. (B) LSVs of Fe₃O₄/rGO/BOD-MGCE under N₂ (a) and O₂ (b) saturated in 0.1 M PBS pH 7.0 at a scan rate of 1 mV/s.

Fig. 10A displays the CVs recorded at Fe $_3$ O $_4$ /rGO/BOD-MGCE in N $_2$ (curve a) and O $_2$ (curve b) saturated 0.1 PBS pH 7.0. It can be seen that the presence of oxygen in the system and a highly enhanced cathodic peak current increase was observed with a peak

potential of oxygen reduction of +0.51 V versus Ag/AgCl. The potential of the peak begins at +0.60 V, whereas the presence of nitrogen in the modified electrodes exhibited no catalytic activity. These results agree with literature data of approximately +0.5 V (vs. Ag/AgCl) [63], which is close to the redox potential of the T1 copper site BOD. It demonstrates that the modified electrode that immobilized BOD has the capability to achieve DET and efficiently catalyze oxygen reduction to water. Linear sweep voltammetry (LSV) was also used to study the electrocatalytics of $Fe_3O_4/rGO/BOD-MGCE.Fig.$ 10B shows the linear sweep voltammograms (LSVs) obtained at $Fe_3O_4/rGO/BOD-MGCE$ in oxygen saturated 0.1 M PBS pH 7. The reduction current increased, indicating that oxygen reduction activity occurred at the $Fe_3O_4/rGO/GOD-MGCE$. As shown in Fig. 10B in curve b, O_2 saturated the current response and showed significant increase by two-fold compared to N_2 saturated (curve a). The biocatalytic appears potential at +0.51 V, indicating BOD was envisaged as the new biocathode of EBC for oxygen reduction in a neutral medium.

$$O_2 + 4H^+ + 4e^- \rightarrow 2H_2O$$
 (6)

16. The performance of EBC

EBC performance was measured with Fe₃O₄/rGO/GOD-MGCE as the bioanode and Fe₃O₄/rGO/BOD-MGCE as the biocathode without a separating membrane, as shown in Fig. 7. The EBC system was operated at 37 °C in 0.1 M PBS pH 7.0 and 5 mM of glucose was used as fuel. At the bioanode, glucose was oxidized by GOD to gluconolactone, where the electrons were transferred from the GOD to the Fe₃O₄/rGO-MGCE. Electrons were flowed through an external circuit then released at the biocathode to BOD, where oxygen was reduced into water. An electrical current is generated as a result of the electrons flow. The cell voltage was measured with a multi-meter under different loads varying from 10 M Ω to 200 Ω applied to the EBC system. The current and power density was calculated from the voltage using ohm's law. Fig. 11 shows two curves of the polarization curve and power density curves of the EBC in the presence of 5 mM glucose, describing the dependence of both open circuit voltage (OCV) and the power density (P) on current density (j) of the bioelectrode based glucose EBC. The OCV of the EBC was around +0.626 V, the maximum current density was 380 µA cm⁻² and the maximum power density was 73.7 µW cm⁻² at +0.38 V which was higher than the glucose EBC reported of V. Krikstolaityte et al., 2013 (3.5 μ W cm⁻²) [64] and A. Ramanavicius et al., 2015 (4.2 µW cm⁻²) [65]. The improvement of power output can be achieved by Fe₃O₄/rGO nanocomposite. The performance of this present glucose EBC is quite comparable and better than some previously reported in literature for mediatorless glucose EBC based on DET in both bioelectrodes, as shown in Table 2. The EBC showed repeatability with an R.S.D of 5.73% for 5 repeatable measurements carried out with the flow system. These results indicate that Fe₃O₄/rGO based nanocomposites can be useful materials for the fabrication of EBC to gain energy from biological fuels such as glucose. Moreover, Fe₃O₄/rGO has great potential for the fabrication of glucose EBC due to operation in the physiological conditions of humans, preparation protocols and simple EBC assembly protocols without mediators or membranes.

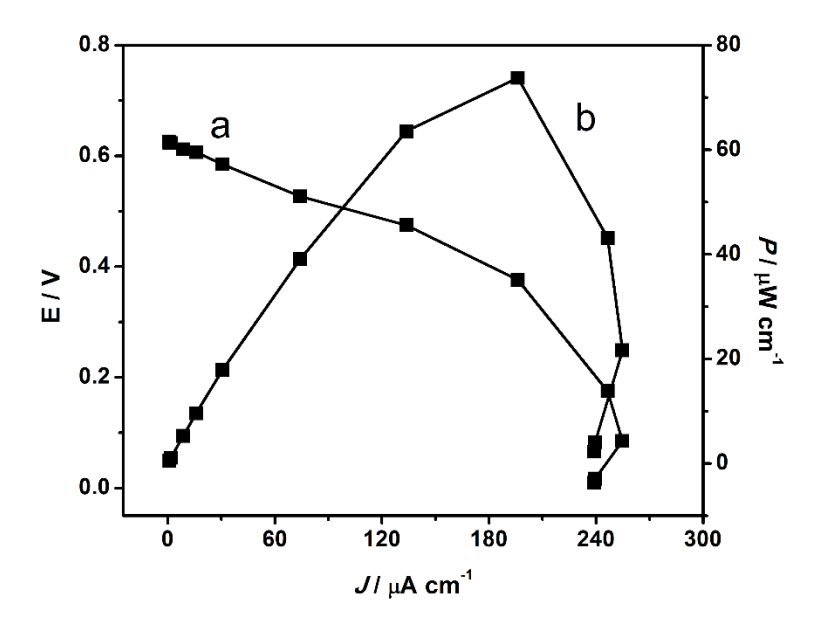


Fig. 11. Polarization curve (a) and power density curve (b) of the mediatorless based glucose EBC on current density in 0.1 M PBS pH 7.0 containing 5 mM glucose under O_2 -saturation.

Table 2. Comparison of glucose EBC based on mediatorless type for both cathode and anode

Modified electrode	Anode	Cathode	OCV	Power density	Glucose	Ref.	
	enzyme	enzyme	(V)	(μ W cm ⁻²)	concentration		
SWNT/pSi	GOD	laccase	-	1.38	4 mM, pH 7	66	
SWNT/PPR: CNP/PPR	GOD	tyrosinase	_	157.4	1 mM, pH 6.5	67	
CNT disks	GOD/	laccase	0.95	1300	5 mM, pH 7	68	
	catalase						
CNTs-IL/CP	GDH	BOD	0.56	13.5	30 mM, pH 7	69	
NPNW	GOD	laccase	0.23	30	-	70	
Graphene/SWNT cogel	GOD	BOD	0.61	190	100 mM, pH 7	71	
CNDs/GC	GOD	BOD	0.93	40.8	4 mM, pH 7.2	63	
CNT-PEI	GOD	laccase	-	102	40 mM, pH 5.5	72	
Fe ₃ O ₄ /rGO/MGCE	GOD	BOD	0.63	73.7	5 mM, pH 7	This	
						work	

CNDs: carbon nanodots; pSi: porous silicon wafer; SWNTs: SWNTs; GOD: glucose oxidase; BOD: bilirubin oxidase; SPGE: spectrographic graphite electrodes; GDH: Glucose dehydrogenase; CNTs-IL: ionic liquid functionalized carbon nanotubes; NPNW: Nafion/poly(vinyl pyrrolidone) compound nanowire; CP: carbon paper; CG: carbon aerogel; CNP: carbon nanopowder; PEI: Poly(ethylenimine); PPR: polypyrrole

17. The stability of EBC

The stability of EBC was characterized by measuring its power loss when continuously working in an air-saturated quiescent buffer containing 5 mM glucose coupling with 1 M Ω of resistance loaded on the cell. The maximum power density was observed for 4 weeks. After operating for 24 h, the power of the EBC retained 98.37 % of its original power output and held steady at 95.39 % after duration of 7 days. Then 78.7 % of initial power density was retained even after 4 weeks, which revealed good durability and stability of the fabricated EBC as shown in Fig. 12. However, the OCV of the EBC remained unchanged during the duration. This could indicate that covalent bonding was unaffected by changes in the surrounding environment. Moreover, the electrostatic interaction binds with enzymes and magnetic force at MGCE to prevent leaching from the electrode surface during operation and storage. In EBC development, the stability of the enzymes on the electrode is the main factor for retaining long-term

performance of the membraneless EBC. However, no significant breakthrough has been achieved in this work concerning the longevity of EBCs.

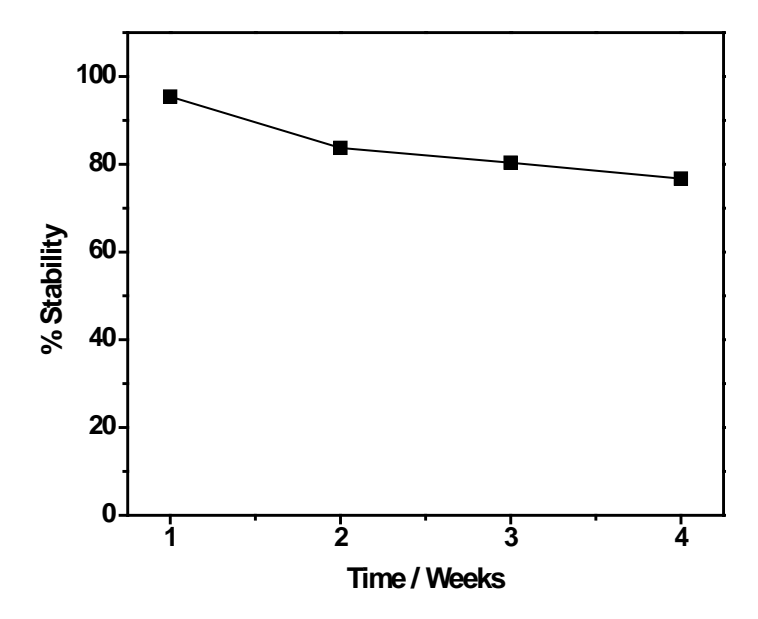


Fig. 12 The stability of the DET-based glucose EBC in 0.1 M PBS pH 7.0 containing 5 mM glucose under O_2 -saturated.

18. Characterization of the graphene and Fe_3O_4 NPs by X-ray absorption spectroscopy and x-ray photoelectron spectroscopy

X-ray absorption spectroscopy and x-ray photoelectron spectroscopy were used to investigate the structure and composition of the prepared samples. XANES spectra were recorded at the energy range of 7125-7128 eV to examine the photo absorption characteristic of Fe atoms (Fig. 13A). Normalized Fe K-edge XANES of functionalized Fe₃O₄ NPs revealed the main absorption peaks at around 7114 eV, 7133 eV and 7146 eV. The first two peaks arose from the electronic transition of 1s \Box d and 1s \Box p states while the third peak was due to the interference of the photoelectron wave. The comparison of XANES spectrum between Fe₃O₄ NPs and the commercial-available iron oxide compounds showed the similarity of Fe₃O₄ NPs and standard Fe₃O₄. Generally, Fe₃O₄ magnetite) has a cubic inverse spinel structure where ferrous (FeO) species occupy half of the octahedral lattice sites and ferric (Fe₂O₃) species are split to occupy the remaining octahedral sites and the tetrahedral sites. Therefore, Fe₃O₄ exhibits the magnetic behavior at room temperature [61]. From XANES results, hence, the structural similarity between Fe₃O₄ NPs and standard Fe₃O₄ suggested its magnetic character. The normalized

Fe K-edge XANES of Fe $_3O_4$ /GO and Fe $_3O_4$ /rGO closely resembled the Fe $_3O_4$ NPs. These results demonstrated that the local structure of Fe $_3O_4$ NPs remained unchanged during the preparation process.

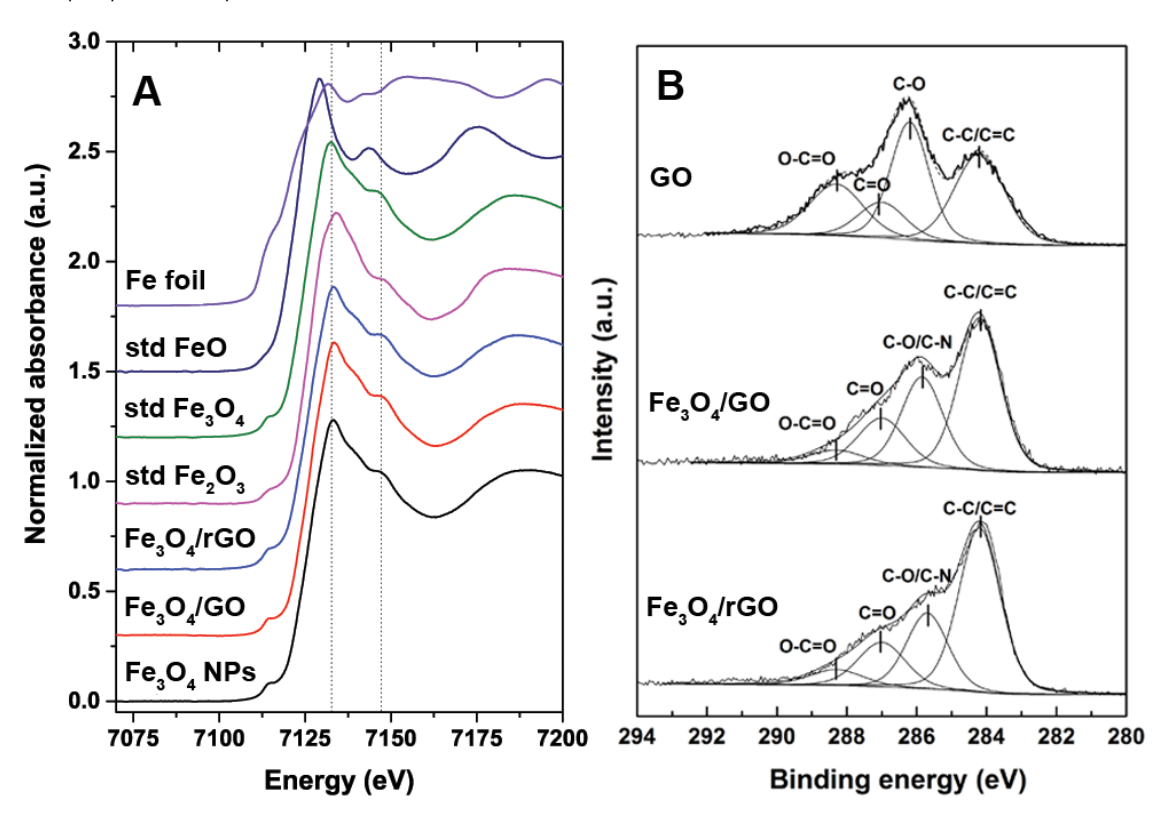


Fig. 13. (A) Normalized Co K-edge spectra of Fe foil, standard FeO, standard Fe₃O₄, standard Fe₂O₃, Fe₃O₄/rGO, Fe₃O₄/GO and Fe₃O₄ NPs, and (B) the C 1s XPS spectra GO, Fe₃O₄/GO and Fe₃O₄/rGO.

X-ray photoelectron spectroscopy was conducted to examine the chemical composition of carbon compounds in the prepared samples. As shown in Fig. 13B, C 1s XPS spectra of GO could be deconvoluted into four peaks corresponding to O-C=O (288.3 eV), C=O (287.0 eV), C=O (286.2 eV), and C-C/C=C (284.2 eV) [74]. To prepare Fe₃O₄/GO, the functionalized Fe₃O₄ was designed to dope on GO surface at the carboxylic group. The reduction of C 1s peak-intensity of the O-C=O group on Fe₃O₄/GO confirmed the reaction. It is known that the presence of oxide-containing species caused the disrupting of the sp² bonding network in graphene and consequently enhanced its electrical resistivity. To improve the electrical conductivity of Fe₃O₄/rGO, glucose-reduction reaction was performed. From C 1s XPS spectra of Fe₃O₄/rGO displayed the reduction of C-O ratio, this

result indicated the removing of oxide-containing species from the GO surface and consequently improved its electrical conductivity.

19. Electrochemical behavior of different modified electrodes

The electrochemical behavior toward RAC detection was investigated using cyclic voltammograms. According to the CV of different modified electrodes, we can observe the oxidation current signal change of these modified electrodes. Fig. 14 exhibits the CV of 1 mM RAC at bare MSPCE (a), Fe₃O₄/GO-MSPCE (b), Fe₃O₄-MSPCE (c) and Fe₃O₄/rGO-MSPCE (d). So the CV of bare MSPCE (curve a) was observed as the lowest oxidation current signal. The Fe₃O₄ NPs modified electrode (curve c) presents a higher current signal response due to the increases specific surface area and enhanced conductibility. It also found that the peak current was decreased at the Fe₃O₄/GO-MSPCE (curve b) due to GO being an insulator material. After modified with Fe₃O₄/rGO (curve d), the peak current significantly enhanced two-fold more than Fe₃O₄/GO with peak potential at 0.686 V. It can be deduced that the graphene structure was reconstructed to aromatic ring after oxygen-containing groups on the surface of GO were removed by the reduction process with glucose. This gain in analytical performance of the Fe₃O₄/rGO may be ascribed to two main factors. One is Fe₃O₄/rGO can increase the conductibility and efficiently enhance the current signal of an electrode. The other can be attributed to the effective surface area enrichment of Fe $_3$ O $_4$ /rGO for the RAC molecules on the electrode surface.

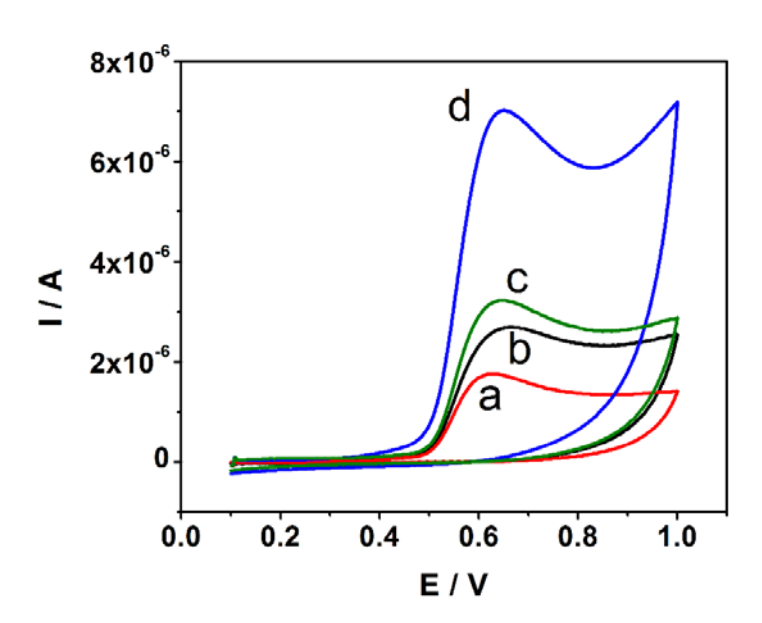


Fig. 14. CV curves of 1 mM RAC at bare MSPCE (a), Fe_3O_4 /GO-MSPCE (b), Fe_3O_4 -MSPCE (c) and Fe_3O_4 /rGO-MSPCE (d) in 0.1 M PBS pH 7.0. Scan rate: 50 mV s⁻¹.

20. Determination of RAC concentration

The DPV was used for the determination of RAC with highly sensitive and low detection limit, under the optimum conditions at a potential range from 0 to 1.0 V. Fig. 15A displayed the DPV signal response for different concentrations of RAC from 0.05 μ M to 250 μ M. As expected, the oxidation peak currents were increased proportionally with the increasing of RAC concentrations, and the resulting calibration plots in Fig. 15B are linear over the range from 0.05 μ M to 10 μ M and 10 μ M to 100 μ M. The corresponding linear regression equations are $I_{\rm p1}(\mu$ A) = 0.1618x + 0.3263 (R² =0.992) and $I_{\rm p2}(\mu$ A) =0.0401x + 1.4046 (R² =9.088), respectively. The detection limit was evaluated to be 13 nM at a signal-to-noise ratio (S/N) of 3. The comparisons of Fe₃O₄/rGO-MSPCE with other modified electrodes for the electrochemical determination of RAC were summarized in Table 3. It can be seen that our proposed sensor in this work shows improved performance of the sensor compared to some of those recently reported electrochemical RAC sensors. Compared with conventional electrodes, our disposable sensors present several advantages as they are highly versatile, user-friendly, cost-effective and can be use in onsite detection.

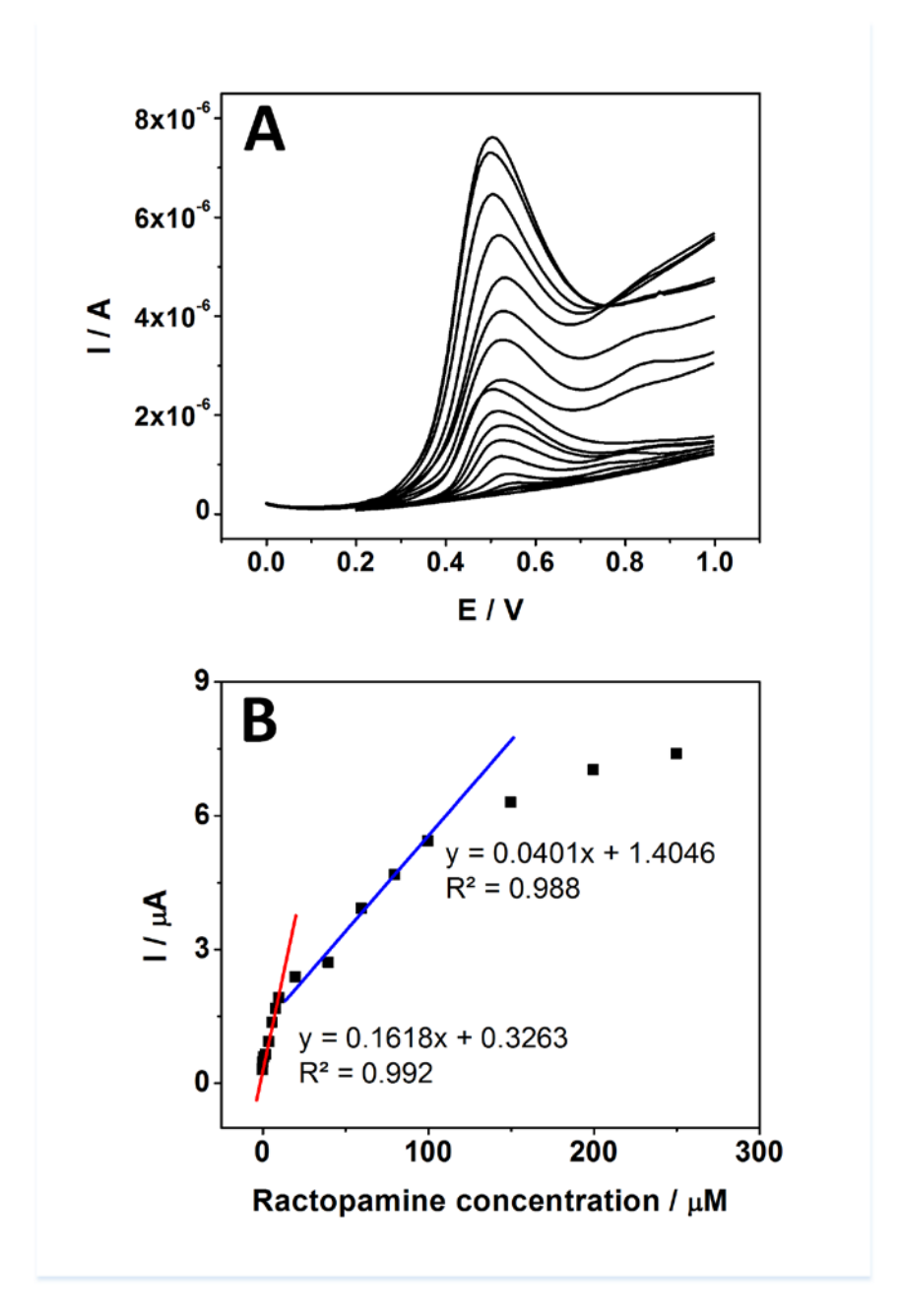


Fig. 15. (A) DPVs of the Fe $_3$ O $_4$ /rGO-MSPE at the RAC concentration from 0.05 μ M to 250 μ M. (B) Calibration curve between the peak current and RAC concentration.

Table 3 Comparison of different material-modified electrodes for RAC detection.

Modified electrode	LOD (nM)	Linear range <u>(μ</u> Μ)	Ref.
GO/GCE	50	0.075 - 3	75
MWCNT-MIM/SPE	6	0.02 - 0.2	76
MWCNT/GCE	59	0.15 - 6	77
poly taurine/ZrO ₂ /GCE	150	1 – 28	78
Gr/GNR	0.51	0.001 - 2.7	79
OMC/GCE	60	0.085 - 8	80
AB/GCE	1.6	0.003 - 6	81
Au/OMC/GCE	4.4	0.03 - 74	82
MIM-Aunps/OMCs/SPE	0.04	0.05 – 1 nM	83
3D MnO ₂ /RGO@nickle foam	11.6	0.017 - 0.962	84
ATONPs/CNTs/GCE	3.3	0.01 - 0.24	85
MCF/CPE	10	0.05-3.0	86
PMEO ₂ MA/C ₆₀ -rGO/GCE	82	0.1-3.1	87
Fe ₃ O ₄ /rGO-MSPE	13	0.05–10,	This work
		10-100	

21. Interference test

The possible coexisting species on RAC detection should not be neglected. Therefore, the effect of interference response on Fe₃O₄/rGO-MSPE was investigated. Fig. 16A showed the current response at Fe₃O₄/rGO-MSPE toward 100 μ M of ascorbic acid (AA), uric acid (UA) and RAC at the potential range from 0 to 1.0 V. Curves c and b exhibit oxidation peak of RAC at 0.587 V and of AA at 0.07 V, respectively, while in curve a, no interference was detected with addition of UA. These results indicated that AA and

UA did not appear to interfere with the determination of RAC at Fe $_3$ O $_4$ /rGO-MSPE and it could be an outstanding candidate to detect RAC in a real sample.

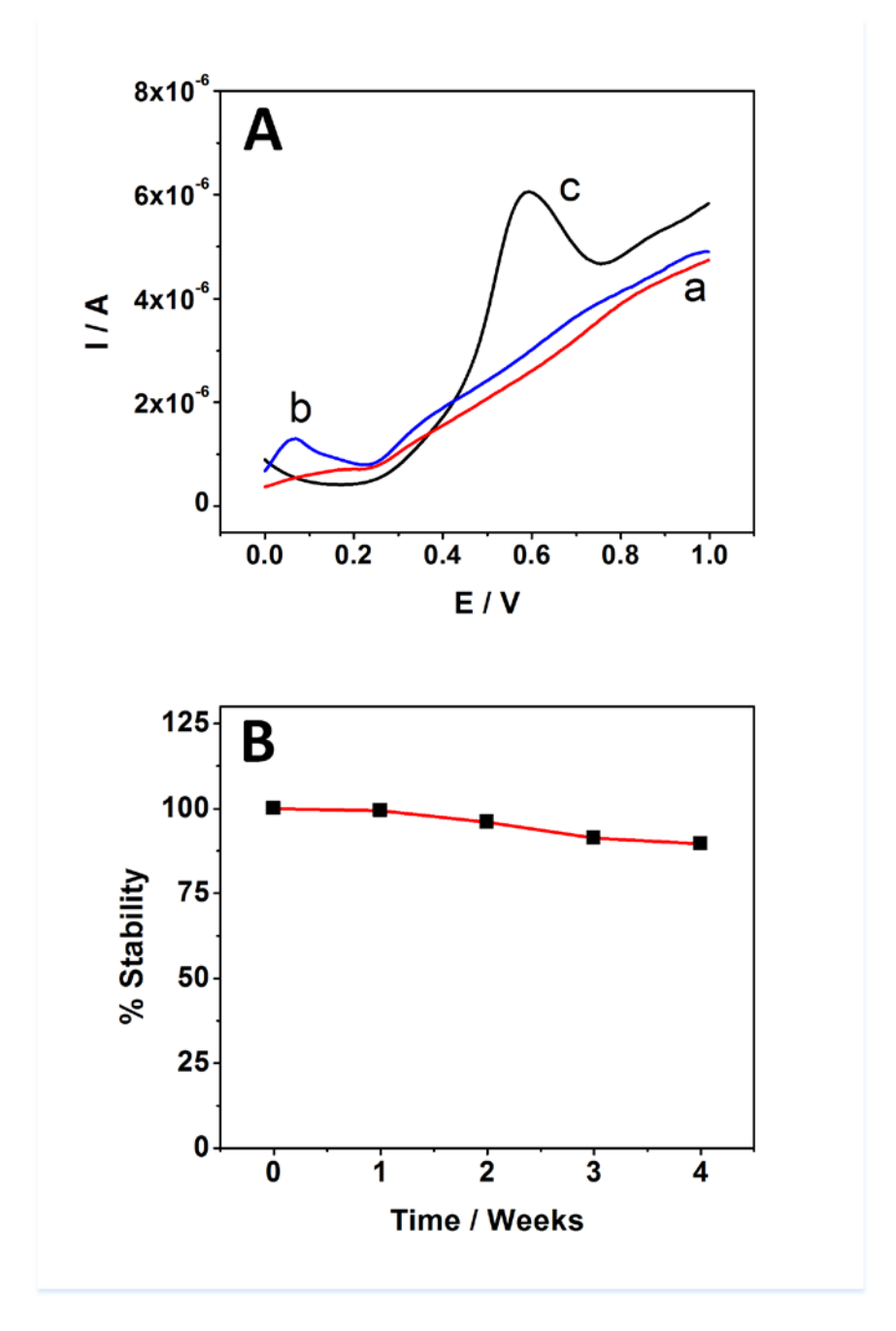


Fig. 16. (A) DPVs of Fe $_3$ O $_4$ /rGO-MSPE in 0.1 M PBS pH 7.0 in the presence of 100 μ M uric acid (UA) (a), 100 μ M ascorbic acid (AA) (b) and 100 μ M RAC (c). (B) The effect of the long term stability.

22. Reproducibility and stability

The sensor can be kept at room temperature. Thus, the stability for the longer period of time of the modified electrode was evaluated. As shown in Fig. 16B, the stability of the sensor was estimated by testing the current response to $100~\mu M$ RAC. After keeping it at room temperature for 4 weeks, the sensor retained about 89.63% of initial response, which indicated that the sensor has good stability. The reproducibility of the current signal of the 15 different electrodes was investigated. The relative standard deviation (RSD) was 1.28% for 15 measurements indicating that the sensor had a good reproducibility.

23. Real samples test

In order to examine the practicability of this sensor in a real sample, it was used for determining the recoveries of RAC in real pork samples. The standard solution of RAC with different concentrations were spiked into the sample, and then analyzed under the same optimal conditions by DPV. The real sample was tested in triplicate by the standard addition method, and the obtained results presented in Table 4. The recovery values of RAC for different real pork samples varied from 90.13% to 109.63% and the RSD is below 6% confirming this proposed sensor was suitable for effective quantitative detection of RAC in real samples.

Table 4. The determination of RAC from the spiked real pork samples (N=3).

Sample	Amount added	Amount found	Recovery (%)	RSD (%)
1	0	0	109.63	5 . 03
	10	10.96	107.03	3.03
2	0	0	90.13	1.81
	50	45.06	70.13	1.01
3	0	0	98.66	2.10
	75	73.99	70.00	2.10
4	0	0	103.93	2,25
	100	103.93	103,73	

Conclusions

This research work successfully demonstrates a design and simple platform for construction of an enzymatic biofuel cell based on direct electron transfer (mediatorless) BFC by Fe₃O₄/rGO/GOD as the bioanode and Fe₃O₄/rGO/BOD as the biocathode. Enzymes were incorporated into Fe₃O₄/RGO by strong electrostatic interaction. The properties of graphene and magnetic nanoparticles enhance enzymatic biofuel cells for more efficient conductivity and also increase the immobilization of enzymes and modified bioelectrodes without the binder or adhesive agents that usually block electron transfers at electrode surfaces. Fe₃O₄ NPs not only increases the surface area, but also has paramagnetic properties which make them more easily manipulated by an external magnetic field to prevent the leakage of enzymes at electrode surfaces. This bioelectrode fabrication approach could offer promising solutions for generations of new classes of membraneless biofuel cells. Moreover, We have successfully prepared an Fe₃O₄/rGO/GOD nanocomposite modified MSPCE by covalent bonding and a GOD was self-assembled with an Fe₃O₄/rGO applied to it for constructing a mediatorless glucose biosensor. An Fe₃O₄/rGO/GOD nanocomposite can provide a unique microenvironment for direct electrochemistry of a GOD immobilized on the surface of a modified electrode, which can retain its high electrocatalytic activities. Additionally, the MSPCE has the advantages of miniaturization, mass production and low cost, thus it is very useful in a disposable measurement for point of care devices. Furthermore, in this research, a simple, novel, low-cost disposable electrochemical sensor for the rapid determination of RAC using Fe₃O₄/rGO nanocomposite was developed. The nanocomposite showed a strong superparamgnetism property which not only aided in facilely adhering the nanocomposite to the electrode surface by magnetically controllable assembling but also made it more stable and improve its electrochemical behavior. The results indicated that the sensor showed good electrochemical characteristics, high stability, sensitivity, acceptable selectivity, reproducibility, easy preparation and low detection limit. This proposed sensor was capable of determining RAC amounts of the actual pork samples with high recoveries. Gradually, the advantages offered by this disposable sensor are drawing more and more attention to this type of sensor technology as an effective device for the development of portable sensors to be used in on-site and real-time electroanalysis.

References

- [1] G. Merle, A. Habrioux, K. Servat, M. Rolland, C. Innocent, K.B. Kokoh, S. Tingry, Long-term activity of covalent grafted biocatalysts during intermittent use of a glucose/O2 biofuel cell, Electrochimica Acta, Vol. 54, 2009, pp. 2998-3003.
- [2] Y. Tan, W. Deng, B. Ge, Q. Xie, J. Huang, S. Yao, Biofuel cell and phenolic biosensor based on acid-resistant laccase–glutaraldehyde functionalized chitosan–multiwalled carbon nanotubes nanocomposite film, Biosensors and Bioelectronics, Vol. 24, 2009, pp. 2225-2231.
- [3] C. Liu, S. Alwarappan, Z. Chen, X. Kong, C.Z. Li, Membraneless enzymatic biofuel cells based on graphene nanosheets, Biosensors and Bioelectronics, Vol. 25, 2010, pp. 1829-1833.
- [4] M. Zhou, L. Deng, D. Wen, L. Shang, L. Jin, S. Dong, Highly ordered mesoporous carbons-based glucose/ O_2 biofuel cell, Biosensors and Bioelectronics, Vol. 24, 2010, pp. 2904-2908.
- [5] E. Simon, C.M. Halliwell, C.S. Toh, A E.G Cass, P.N. Bartlett, Immobilisation of enzymes on poly(aniline)—poly(anion) composite films. Preparation of bioanodes for biofuel cell applications, Bioelectrochemistry, Vol. 55, 2002, pp. 13-15.
- [6] D. Ivnitski, B. Branch, P. Atanassov, C. Apblett, Glucose oxidase anode for biofuel cell based on direct electron transfer, Electrochemistry Communications, Vol. 8, 2006, pp. 1204-1210.
- [7] A. Zebda, C. Gondran, A. L. Goff, M. Holzinger, P. Cinquin, S. Cosnier, Mediatorless high-power glucose biofuel cells based on compressed carbon nanotube-enzyme electrodes, Nature Communications, Vol 2, 2011, Article number: 370.
- [8] V. Mani, R. Devasenathipathy, S. M. Chen, J. A. Gu, S. T. Huang, Synthesis and characterization of graphene-cobalt phthalocyanines and graphene-iron phthalocyanine composites and their enzymatic fuel cell application, Renewable Energy, Vol 74, 2015, pp. 867-874.
- [9] B. Devadas, V. Mani, S.M. Chen, A Glucose/O2 Biofuel Cell Based on Graphene and Multiwalled Carbon Nanotube Composite Modified Electrode, International Journal of Electrochemical science, Vol 7, 2012, pp. 8064 8075.
- [10] F. Xia, D.B. Farmer, Y.M. Lin, P. Avouris, Graphene Field-Effect Transistors with High On/Off Current Ratio and Large Transport Band Gap at Room Temperature, Nano Letter, Vol. 10, 2010, pp. 715-718.

- [11] G. Ko, H.Y. Kim, J. Ahn, Y.M. Park, K.Y. Lee, J. Kim, Graphene-based nitrogen dioxide gas sensors, Current Applied Physics, Vol. 10, 2010, pp. 1002-1004.
- [12] H.J. Yoon, D.H. Jun, J.H. Yang, Z. Zhou, S.S. Yang, M.M.-C. Cheng, Carbon dioxide gas sensor using a graphene sheet, Sensors Actuators B: Chem., Vol. 157, 2011, pp. 310-313.
- [13] T. Kuila, S. Bose, P. Khanra, A.K. Mishra, N.H. Kim, J.H. Lee, Recent advances in graphene-based biosensors, Biosens. Bioelectron., Vol. 26, 2011, pp. 4637-4648.
- [14] M. Pumera, A. Ambrosi, A. Bonanni, E. L. K. Chng, H. L. Poh, Graphene for electrochemical sensing and biosensing, TrAC Trends in Analytical Chemistry, Vol. 29, 2010, pp. 954-965.
- [15] Y. Shao, J. Wang, H. Wu, J. Liu, I.A. Aksay, Y. Lin, Graphene Based Electrochemical Sensors and Biosensors: A Review, Electroanalysis, Vol. 22, 2010, pp. 1027-1036.
- [16] C. Berger, Z. Song, T. Li, X. Li, A.Y. Ogbazghi, R. Feng, Z. Dai, A.N. Marchenkov, E.H. Conrad, P. N. First, W. A. de Heer, Ultrathin epitaxial graphite: 2D electron gas properties and a route toward graphene-based nanoelectronics, The Journal of Physical Chemistry B, Vol. 108, 2004, pp. 19912-19916.
- [17] M. Liang, L. Zhi, Graphene-based electrode materials for rechargeable lithium batteries, Journal of Materials Chemistry, Vol. 19, 2009, pp. 5871-5878.
- [18] G. Wang, X. Shen, J. Yao, J. Park, Graphene nanosheets for enhanced lithium storage in lithium ion batteries, Carbon, Vol. 47, 2009, pp. 2049-2053.
- [19] J.J. Yoo, K. Balakrishnan, J. Huang, V. Meunier, B.G. Sumpter, A. Srivastava, M. Conway, A.L. Mohana Reddy, J. Yu, R. Vajtai, P.M. Ajayan, Ultrathin Planar Graphene Supercapacitors, Nano Letter, Vol. 11, 2011, pp. 1423-1427.
- [20] L. Wang, K. Lee, Y.-Y. Sun, M. Lucking, Z. Chen, J.J. Zhao, S.B. Zhang, Graphene oxide as an ideal substrate for hydrogen storage, ACS Nano, Vol. 3, 2009, pp. 2995-3000.
- [21] Y.P. He, Q.L. Sheng, J.B. Zheng, M.Z. Wang, B. Liu, Magnetite-graphene for the direct electrochemistry of hemoglobin and its biosensing application. Electrochimica Acta, Vol 56, 2011, pp. 2471–2476.
- [22] D. Lu, Y. Zhang, L. Wang, S.X. Lin, C.M. Wang, X.F. Chen, Sensitive detection of acetaminophen based on Fe3O4 nanoparticles-coated poly(diallyldimethylammonium chloride) functionalized graphene nanocomposite film, Talanta, Vol 88, 2012, pp. 181–186.
- [23] A. Lerf, H. He, M. Forster, J. Klinowski, Structure of Graphite Oxide Revisited, The Journal of Physical Chemistry B, Vol 102, 1998, pp. 4477–4482.

- [24] S. Stankovich, R.D. Piner, X. Chen, N. Wu, S.T. Nguyen, R.S. Ruoff, Stable Aqueous Dispersions of Graphitic Nanoplatelets via the Reduction of Exfoliated Graphite Oxide in the Presence of Poly(sodium 4-styrenesulfonate), Journal of Materials Chemistry, Vol 16, 2006, pp. 155–158.
- [25] S. Stankovich, D.A. Dikin, R.D. Piner, K.A. Kohlhaas, A. Kleinhammes, Y. Jia, Y. Wu, S.T. Nguyen, R.S. Ruoff, Synthesis of graphene-based nanosheets via chemical reduction of exfoliated graphite oxide, Carbon, Vol 45, 2007, pp. 1558–1565.
- [26] C. Zhu, S. Guo, Y. Fang, S. Dong, Reducing Sugar: New Functional Molecules for the Green Synthesis of Graphene Nanosheets, ACS Nano, Vol 4, 2010, pp. 2429–2437.
- [27] C.H. Dodd, H.C. Hsu, W.J. Chu, P. Yang, H.G. Zhang, J.D. Mountz Jr., K. Zinn, J. Forder, L. Josephson, R. Weissleder, J.M. Mountz, J.D. Mountz, Normal T-cell response and in vivo magnetic resonance imaging of T cells loaded with HIV transactivator-peptide-derived superparamagnetic nanoparticles, Journal of Immunological Methods, Vol. 256, 2001, pp. 89-105.
- [28] M. Arruebo, R.F. Pacheco, M.R. Ibarra, J. Santamaría, Magnetic nanoparticles for drug delivery, Nano Today, Vol. 2, 2007, pp. 22-32.
- [29] T. Szabo, A. Bakandritsos, V. Tzitzios, E. Devlin, D. Petridis, I. Dekany, Magnetically modified single and turbostratic stacked graphenes from tris(2,20-bipyridyl) iron(II) ionexchanged graphite oxide. The Journal of Physical Chemistry B, Vol 112, 2008, pp. 14461–14469.
- [30] Y. Jiang, C. Guo, H. Xia, I. Mahmood, C. Liu, H. Liu, Magnetic nanoparticles supported ionic liquids for lipase immobilization: Enzyme activity in catalyzing esterification, Journal of Molecular Catalysis B: Enzymatic, Vol. 58, 2009, pp. 103-109.
- [31] J. D. Qiu, H. P. Peng R. P. Liang, X. H. Xia, Facile preparation of magnetic core-shell Fe3O4@Au nanoparticle/myoglobin biofilm for direct electrochemistry, Biosensors and Bioelectronics, Vol 25, 2010, pp. 1447-1453.
- [32] H. P. Peng, R. P. Liang, J. D. Qiu, Facile synthesis of Fe3O4@Al2O3 core-shell nanoparticles and their application to the highly specific capture of heme proteins for direct electrochemistry, Biosensors and Bioelectronics, Vol 26, 2011, pp. 3005-3011.
- [33] C. Zou, Y. Fu, Q. Xie, S. Yao, High performance glucose amperometric biosensor based on magnetic polymeric bionanocomposites, Biosensors and Bioelectronics, Vol 25, 2010, pp. 1277-1282.

- [34] S. Wu, H. Wang, S. Tao, C. Wang, L. Zhang, Z. Liu, C. Meng, Magnetic loading of tyrosinase- Fe3O4/ mesoporous silica core/ shell microspheres for high sensitive electrochemical biosensing", Analytica Chimica Acta, Vol 686, 2011, pp. 81-86.
- [35] J. Shen, Y. Hu, M. Shi, N. Li, H. Ma, M. Ye, One Step Synthesis of Graphene oxide–magnetic nanoparticle composite, The Journal of Physical Chemistry C, Vol. 114, 2010, pp. 1498-1503.
- [36] X. Yang, X. Zhang, Y. Ma, Y. Huang, Y. Wang, Y. Chen, Superparamagnetic graphene oxide–Fe₃O₄ nanoparticles hybrid for controlled targeted drug carriers, Journal of Materials Chemistry, Vol. 19, 2009, pp. 2710-2714.
- [37] Q. Wu, G. Zhao, C. Feng, C. Wang, Z. Wang, Preparation of a graphene-based magnetic nanocomposite for the extraction of carbamate pesticides from environmental water samples, Journal of Chromatography A, Vol. 1218, 2011, pp. 7936-7942.
- [38] F. He, J. Fan, D. Ma, L. Zhang, C. Leung, H. L. Chan, The attachment of Fe_3O_4 nanoparticles to graphene oxide by covalent bonding, Carbon, Vol 48, 2010, pp.3139 –3144.
- [39] M. E. Turberg, J. M. Rodewald, M. R. Coleman, Determination of ractopamine in monkey plasma and swine serum by high-performance liquid chromatography with electrochemical detection, Journal of Chromatography B, Vol 675, 1996, pp. 279–285.
- [40] L.E. Watkins, D.J. Jones, D.H. Mowrey, D.B. Andersom, E.L. Veenhuizen, The effect of various levels of ractopamine hydrochloride on the performance and carcass characteristics of finishing swine, Journal of Animal Science, Vol 68, 1990, pp. 3588-3595
- [41] E. Shishani, S. C. Chai, S. Jamokha, G. Aznar, M. K. Hoffman, Determination of ractopamine in animal tissues by liquid chromatography-fluorescence and liquid chromatography/ tandem mass spectrometry, Analytica Chimica Acta, Vol. 483, 2003, pp. 137–145.
- [42] X. Lu, H. Zheng, X.Q. Li, X.X. Yuan, H. Li, L.G. Deng, Detection of ractopamine residues in pork by surface plasmon resonance-based biosensor inhibition immunoassay, Food Chemistry, Vol 130, 2012, pp. 1061-1065.
- [43] [33] F. Zhang, J. Jin, X. Zhong, S. Li, J. Niu, R. Li, J. Ma, Pd immobilized on amine-functionalized magnetite nanoparticles: a novel and highly active catalyst for hydrogenation and Heck reactions, Green Chemistry, 13 (2011) 1238-1243.

- [44] H. Ni, X. Sun, Y. Li, C. Li, Solvothermal self-assembly of magnetic Fe₃O₄ nanochains by ethylenediamine functionalized nanoparticles for chromium (VI) removal, Journal of Materials Science, 50 (2015) 4270-4279.
- [45] S. Bahar, F. Karami, Amino-functionalized Fe_3O_4 –graphene oxide nanocomposite as magnetic solid-phase extraction adsorbent combined with flame atomic absorption spectrometry for copper analysis in food samples, Journal of the Iranian Chemical Society, 12 (2015) 2213-2220.
- [46] F. He, J. Fan, D. Ma, L. Zhang, C. Leung, H.L. Chan, The attachment of Fe₃O₄ nanoparticles to graphene oxide by covalent bonding, Carbon, 48 (2010) 3139-3144.
- [47] C. Zhu, S. Guo, Y. Fang, S. Dong, Reducing sugar: new functional molecules for the green synthesis of graphene nanosheets, ACS nano, 4 (2010) 2429-2437.
- [48] Z.-J. Fan, W. Kai, J. Yan, T. Wei, L.-J. Zhi, J. Feng, Y.-m. Ren, L.-P. Song, F. Wei, Facile synthesis of graphene nanosheets via Fe reduction of exfoliated graphite oxide, ACS nano, 5 (2010) 191-198.
- [49] Y. Liu, M. Wang, F. Zhao, Z. Xu, S. Dong, The direct electron transfer of glucose oxidase and glucose biosensor based on carbon nanotubes/chitosan matrix, Biosensors and Bioelectronics, 21 (2005) 984-988.
- [50] E. Laviron, General expression of the linear potential sweep voltammogram in the case of diffusionless electrochemical systems, Journal of Electroanalytical Chemistry and Interfacial Electrochemistry, 101 (1979) 19-28.
- [51] J. Yu, J. Tu, F. Zhao, B. Zeng, Direct electrochemistry and biocatalysis of glucose oxidase immobilized on magnetic mesoporous carbon, Journal of Solid State Electrochemistry, 14 (2010) 1595-1600.
- [52] Q. Liu, X. Lu, J. Li, X. Yao, J. Li, Direct electrochemistry of glucose oxidase and electrochemical biosensing of glucose on quantum dots/carbon nanotubes electrodes, Biosensors and Bioelectronics, 22 (2007) 3203-3209.
- [53] K.H. Hyun, S.W. Han, W.-G. Koh, Y. Kwon, Fabrication of biofuel cell containing enzyme catalyst immobilized by layer-by-layer method, Journal of Power Sources, 286 (2015) 197-203.
- [54] F. Shu, G. Wilson, Rotating ring-disk enzyme electrode for surface catalysis studies, Analytical Chemistry, 48 (1976) 1679-1686.
- [55] Z.O. Araci, A.F. Runge, W.J. Doherty, S.S. Saavedra, Correlating molecular orientation distributions and electrochemical kinetics in subpopulations of an

- immobilized protein film, Journal of the American Chemical Society, 130 (2008) 1572-1573.
- [56] L. Yang, X. Ren, F. Tang, L. Zhang, A practical glucose biosensor based on Fe₃O₄ nanoparticles and chitosan/nafion composite film, Biosensors and Bioelectronics, 25 (2009) 889-895.
- [57] T.-H. Yang, C.-L. Hung, J.-H. Ke, J.-M. Zen, An electrochemically preanodized screen-printed carbon electrode for achieving direct electron transfer to glucose oxidase, Electrochemistry Communications, 10 (2008) 1094-1097.
- [58] H.-P. Peng, R.-P. Liang, L. Zhang, J.-D. Qiu, Facile preparation of novel core–shell enzyme–Au–polydopamine–Fe₃O₄ magnetic bionanoparticles for glucose sensor, Biosensors and Bioelectronics, 42 (2013) 293-299.
- [59] L. Yu, H. Wu, B. Wu, Z. Wang, H. Cao, C. Fu, N. Jia, Magnetic Fe₃O₄-Reduced Graphene Oxide Nanocomposites-Based Electrochemical Biosensing, Nano-Micro Letters, 6 (2014) 258-267.
- [60 S. Zuo, Y. Teng, H. Yuan, M. Lan, Direct electrochemistry of glucose oxidase on screen-printed electrodes through one-step enzyme immobilization process with silica sol–gel/polyvinyl alcohol hybrid film, Sensors and Actuators B: Chemical, 133 (2008) 555-560.
- [61] J. Li, R. Yuan, Y. Chai, Simple construction of an enzymatic glucose biosensor based on a nanocomposite film prepared in one step from iron oxide, gold nanoparticles, and chitosan, Microchimica Acta, 173 (2011) 369-374.
- [62] C. Karuppiah, S. Palanisamy, S.-M. Chen, V. Veeramani, P. Periakaruppan, Direct electrochemistry of glucose oxidase and sensing glucose using a screen-printed carbon electrode modified with graphite nanosheets and zinc oxide nanoparticles, Microchimica Acta, 181 (2014) 1843-1850.
- [63] Zhao, M., Gao, Y., Sun, J. & Gao, F. Mediatorless Glucose Biosensor and Direct Electron Transfer Type Glucose/Air Biofuel Cell Enabled with Carbon Nanodots. *Analytical Chemistry* **87**, 2615-2622, **(**2015**)**.
- [64] Krikstolaityte, V. et al. Biofuel cell based on anode and cathode modified by glucose oxidase. Electroanalysis 25, 2677-2683, (2013).
- [65] Ramanavicius, A. *et al.* Biofuel cell based on glucose oxidase from Penicillium funiculosum 46.1 and horseradish peroxidase. *Chemical Engineering Journal* 264, 165-173, (2015).

- [66] Wang, S. C. et al. Membrane-less and mediator-free enzymatic biofuel cell using carbon nanotube/porous silicon electrodes. Electrochemistry Communications 11, 34-37, (2009).
- [67] Min, K., Ryu, J. H. & Yoo, Y. J. Mediator-free glucose/O₂ biofuel cell based on a 3-dimensional glucose oxidase/SWNT/polypyrrole composite electrode.

 Biotechnology and Bioprocess Engineering 15, 371-375, (2010).
- [68] Zebda, A. *et al.* Mediatorless high-power glucose biofuel cells based on compressed carbon nanotube-enzyme electrodes. *Nature Communications* **2**, 370, (2011).
- [69] Zhang, L. et al. Small-size biofuel cell on paper. Biosensors and Bioelectronics 35, 155-159, (2012).
- [70] Pan, C. *et al.* Generating Electricity from Biofluid with a Nanowire-Based Biofuel Cell for Self-Powered Nanodevices. *Advanced Materials* **22**, 5388-5392, **(**2010**)**.
- [71] Campbell, A. S. *et al.* Membrane/Mediator-Free Rechargeable Enzymatic Biofuel Cell Utilizing Graphene/Single-Wall Carbon Nanotube Cogel Electrodes. *ACS Applied Materials & Interfaces* **7**, 4056-4065, **(**2015**)**.
- [72] Christwardana, M., Kim, K. J. & Kwon, Y. Fabrication of Mediatorless/Membraneless Glucose/Oxygen Based Biofuel Cell using Biocatalysts Including Glucose Oxidase and Laccase Enzymes. *Scientific Reports* 6, 30128, (2016).
- [73] S. Rajput, C. U. Pittman Jr., D. Mohan, Magnetic magnetite (Fe3O4) nanoparticle synthesis and applications for lead (Pb2+) and chromium (Cr6+) removal from water, J. Colloid Interface Sci., 468 (2016) 334-346.
- [74] A. H. Soeriyadi, B. Gupta, P. J. Reecec, J. J. Gooding, Optimising the enzyme response of a porous silicon photonic crystal via the modular design of enzyme sensitive polymers, Polym. Chem., 5 (2014) 2333-2341.
- [75] C. Wu, D. Sun, Q. Li, K. Wu, Electrochemical sensor for toxic ractopamine and clenbuterol based on the enhancement effect of graphene oxide, Sens. Actuators, B, 168 (2012) 178–184.
- [76] H. Zhang, G. Liu, C. Chai, A novel amperometric sensor based on screen-printed electrode modified with multi-walled carbon nanotubes and molecularly imprinted membrane for rapid determination of ractopamine in pig urine, Sensors Actuators B Chem. 168 (2012) 103–110.

- [77] Z. Liu, Y. Zhou, Y. Wang, Q. Chen, K. Wu, Enhanced oxidation and detection of toxic ractopamine using carbon nanotube film-modified electrode, Electrochim. Acta, 74 (2012) 139-144.
- [78] M. Rajkumar, Y. S. Li, S. M. Chen, Electrochemical detection of toxic ractopamine and salbutamol in pig meat and human urine samples by using poly taurine/zirconia nanoparticles modified electrodes, Colloids Surf. B, 110 (2013) 242-247.
- [79] W. Bai, H. Huang, Y. Li, H. Zhang, B. Liang, R. Guo, L. Du, Z. Zhang, Direct preparation of well-dispersed graphene/gold nanorod composites and their application in electrochemical sensors for determination of ractopamine, Electrochim. Acta, 117 (2014) 322–328.
- [80] X. Yang, B. Feng, P. Yang, Y. Ding, Y. Chen, J. Fei, Electrochemical determination of toxic ractopamine at an ordered mesoporous carbon modified electrode, Food Chem., 145 (2014) 619-624.
- [81] R. Wang, K. Wu, C. Wu, Highly sensitive electrochemical sensor for toxic ractopamine based on the enhancement effect of acetylene black nanoparticles, Anal. Methods, 7 (2015) 8069–8077.
- [82] Q. Wei, Q. Wang, H. Wang, H. Gu, Q. Zhang, X. Gao, B. Qi, Formation of flowerlike gold nanostructure on ordered mesoporous carbon electrode and its application in electrochemical determination of ractopamine, Mater. Lett., 147 (2015) 58-60.
- [83] M. Ma, P. Zhu, F. Pi, J. Ji, X. Sun, A disposable molecularly imprinted electrochemical sensor based on screen-printed electrode modified with ordered mesoporous carbon and gold nanoparticles for determination of ractopamine, J. Electroanal. Chem., 775 (2016) 171-178.
- [84] M. Y. Wang, W. Z. Zhu, L. Ma, J. J. Ma, D. E. Zhang, Z. W. Tong, J. Chen, Enhanced simultaneous detection of ractopamine and salbutamol via electrochemical-facial deposition of MnO2 nanoflowers onto 3D RGO/Ni foam templates, Biosens. Bioelectron., 78 (2016) 259-266.
- [85] A. K. Baytak, T. Teker, S. Duzmen, M. Aslanoglu, A novel voltammetric sensor based on carbon nanotubes and nanoparticles of antimony tin oxide for the determination of ractopamine, Mater. Sci. and Eng., C, 59 (2016) 368–374.
- [86] L. Xie, Y. Ya, L. Wei, Mesopores cellular foam-based electrochemical sensor for sensitive determination of ractopamine, Int. J. Electrochem. Sci., 12 (2017) 9714–9724.

[87] C. Chen, M. Zhang, C. Li, Y. Xie, J. Fei, Switched voltammetric determination of ractopamine by using a temperature-responsive sensing film, Microchimica Acta 185 (2018) 155.

Output ที่ได้จากโครงการวิจัย

- 1. ผลงานตีพิมพ์ในวารสารวิชาการนานาชาติ
 - 1. Y. Poo-arporn, S. Pakapongpan, N. Chanlek, **R. P. Poo-arporn***, The development of disposable electrochemical sensor based on Fe₃O₄-doped reduced graphene oxide modified magnetic screen-printed electrode for ractopamine determination in pork sample, Sensors & Actuators: B. Chemical, (2019) 284pp. .171–164

 IF667.5=2017 Q1
 - S. Pakapongpan, A. Tuantranont, R. P. Poo-arporn*, Magnetic nanoparticle-reduced graphene oxide nanocomposite as a novel bioelectrode for mediatorless-membraneless glucose enzymatic biofuel cells. Scientific Reports, 7 (2017) 12882
 IF2016=4.259 Q1
 - 3. S. Pakapongpan, **R. P. Poo-arporn***, Self-assembly of glucose oxidase on reduced graphene oxide-magnetic nanoparticles nanocomposite-based direct electrochemistry for reagentless glucose biosensor, Materials science & engineering. C, Materials for biological applications,76 (2017) pp. 398-405. IF2016=4.164 Q2
 - 4. **R.P Poo-arporn***, S. Pakapongpan, P. Khownarumit, D. Waraho-Zhmayev, Y. Poo-arporn, W. Surareungchai, Development of Mevalonic Acid Biosensor using Amperometric Technique Based on Nanocomposite of Nicotinamide Adenine Dinucleotide and Carbon Nanotubes, Journal of The Electrochemical Society, 164 (2017) B349-B355. IF2016=3.259 Q2
- 2. การเสนอผลงานในที่ประชุมวิชาการ
 - 1. Y. Poo-arporn, S. Pakapongpan, R.P. Poo-arporn*, Development of electrochemical sensor based on graphene nanocomposite for determination of β -agonists, In the Proceeding of the 17th International Meeting on Chemical Sensors (IMCS 2018), July 15-19, 2018, University of Vienna, Austria, 709-710

สัญญาเลขที่ RSA5980073

ภาคผนวก

A. Publication

Title: The development of disposable electrochemical sensor based on Fe_3O_4 -doped reduced graphene oxide modified magnetic screen-printed electrode for ractopamine determination in pork sample

Y. Poo-arporn, S. Pakapongpan, N. Chanlek, R. P. Poo-arporn*,

(Sensors & Actuators: B. Chemical, 284 (2019) pp. 164–171) IF2017=5.667 Q1



Title: Magnetic nanoparticle-reduced graphene oxide nanocomposite as a novel bioelectrode for mediatorless-membraneless glucose enzymatic biofuel cells

S. Pakapongpan, A. Tuantranont, R. P. Poo-arporn*

(Scientific Reports, 7 (2017) 12882) IF2016=4.259 Q1

สัญญาเลขที่ RSA5980073

Title: Self-assembly of glucose oxidase on reduced graphene oxide-magnetic nanoparticles nanocomposite-based direct electrochemistry for reagentless glucose biosensor

S. Pakapongpan, R. P. Poo-arporn*

(Materials science & engineering. C, Materials for biological applications, 76 (2017) pp. 398-405.) IF2016=4.164 Q2

สัญญาเลขที่ RSA5980073

Title: Development of Mevalonic Acid Biosensor using Amperometric Technique Based on Nanocomposite of Nicotinamide Adenine Dinucleotide and Carbon Nanotubes

R.P Poo-arporn*, S. Pakapongpan, P. Khownarumit, D. Waraho-Zhmayev, Y. Poo-arporn, W. Surareungchai

(Journal of The Electrochemical Society, 164, (2017), B349-B355.) IF2016=3.259 Q2

B. Proceeding

Title: Development of electrochemical sensor based on graphene nanocomposite $\text{for determination of } \beta\text{-agonists}$

Y. Poo-arporn, S. Pakapongpan, R.P. Poo-arporn*

(In the Proceeding of the 17th International Meeting on Chemical Sensors (IMCS 2018), July 15-19, 2018, University of Vienna, Austria, 709-710)

การเชื่อมโยงกับต่างประเทศหรือรางวัลที่ได้รับ

- 1. 01.05.17-30.05.17: Ernst Mach-Nachbetreuungsstipendium (EZA), Grant/Scholarship Award, Institute of Physical Chemistry, Department of Chemistry, University of Vienna, Vienna, Austria, provided by the Federal Ministry of Science, Research and Economy (BMWFW), Austria
- 2. 24th Science and Technology Research Grant, Thailand Toray Science Foundation, 2017